

Accepted for publication in the Astrophysical Journal

# A New Look at the Binary Characteristics of Massive Stars

Henry A. Kobulnicky

*Department of Physics & Astronomy, University of Wyoming, Laramie, WY 82070*

`chipk@uwyd.edu`

Chris L. Fryer

*Theoretical Astrophysics, Los Alamos National Laboratory, P.O. Box 1663, Los Alamos  
NM 87545*

`fryer@lanl.gov`

## ABSTRACT

We constrain the properties of massive binaries by comparing radial velocity data on 114 early-type stars in the Cygnus OB2 Association with the expectations of Monte Carlo models. Our comparisons test several popular prescriptions for massive binary parameters while highlighting the sensitivity of the best-fitting solutions to the adopted boundary conditions. We explore a range of true binary fraction,  $F$ , a range of power-law slopes,  $\alpha$ , describing the distribution of companion masses between the limits  $q_{low}$  and 1, and a range of power-law slopes,  $\beta$ , describing the distribution of orbital separations between the limits  $r_{in}$  and  $r_{out}$ . We also consider distributions of secondary masses described by a Miller-Scalo type initial mass function (IMF) and by a two-component IMF that includes a substantial “twin” population with  $M_2 \simeq M_1$ . Several seemingly disparate prescriptions for massive binary characteristics can be reconciled by adopting carefully chosen values for  $F$ ,  $r_{in}$ , and  $r_{out}$ . We show that binary fractions  $F < 0.7$  are less probable than  $F \geq 0.8$  for reasonable choices of  $r_{in}$  and  $r_{out}$ . Thus, the true binary fraction is high. For  $F = 1.0$  and a distribution of orbital separations near the canonical Öpik’s Law distribution (i.e., flat;  $\beta = 0$ ), the power law slope of the mass ratio distribution is  $\alpha = -0.6 - 0.0$ . For  $F \simeq 0.8$ ,  $\alpha$  is somewhat larger, in the range  $-0.4 - 1.0$ . In any case, the secondary star mass function is inconsistent with a Miller-Scalo -like IMF unless the lower end is truncated below  $\sim 2-4 M_\odot$ . In other words, massive stars preferentially have massive companions.

The best fitting models are described by a Salpeter or Miller-Scalo IMF for 60% of secondary star masses with the other  $\sim 40\%$  of secondaries having  $M_2 \simeq M_1$ , i.e., “twins”. These best-fitting model parameters simultaneously predict the fraction of type Ib/c supernovae to be 30–40% of all core-collapse supernovae, in agreement with recent observational estimates.

*Subject headings:* techniques: radial velocities — (stars:) binaries: general — (stars:) binaries: spectroscopic — stars: early-type — stars: supernovae — gamma rays: bursts — X-rays: binaries —

## 1. Introduction

### 1.1. Significance and Theoretical Parameterizations of Binaries

Massive binary stars are invoked as the progenitors of a wide variety of astrophysical phenomena, from short and long gamma-ray bursts (Fryer et al. 1999), type Ib/c and blue type II supernovae (Podsiadlowski 1992), to the fastest runaway O/B stars (Blaauw 1961) and the entire menagerie of binary systems with compact remnants: X-ray binaries, millisecond pulsar systems, and double neutron star systems (see Fryer et al. (1998) for a review). Whether binaries are necessary for the formation of all such objects is a matter of debate. For instance, although many authors propose that type Ib/c supernovae and short- and long-duration gamma-ray bursts are produced in binaries, it is still argued that their progenitors may be single stars (Hirschi et al. 2005). Observational studies can contribute to this debate by measuring the frequency, separations, and mass ratios of close massive binary systems.

Although debates on the role of binaries continue, it is generally agreed that most of the progenitors of X-ray binaries and double neutron star binaries in the Galactic disk must arise from massive binary systems. Population synthesis models of these systems, however, adopt very different properties for the progenitors’ stellar components. These studies begin with four assumptions regarding the binary characteristics: the distribution of primary masses, the distribution of secondary masses, the distribution of orbital separations, and the distribution of eccentricities. Population synthesis studies all choose some analytic form for these distributions, generally basing them upon observational constraints on the initial and final binary system parameters.

One significant source of disagreement in these initial distributions is the choice of the secondary star mass function. Typically, the primary star mass distribution is chosen using a field initial mass function (IMF) (e.g., Scalo 1986; Salpeter 1955). The secondary mass can

be chosen through the same IMF or, more commonly, from a distribution of the secondary-to-primary mass ratios:  $f(q)$ , where  $q \equiv M_2/M_1$ . In this latter formalism, the distribution is chosen to be proportional to the mass ratio to some power:  $f(q) \propto q^\alpha$  between the limits  $q_{low} < q < 1.0$ . Note that the power-law slope,  $\alpha$ , is not equivalent to the power-law slope,  $\gamma$ , of the secondary star mass distribution, commonly expressed  $f(M_2) \propto M_2^\gamma$ . The relationship between  $f(q)$  and  $f(M_2)$  is discussed by Tout (1991), and it is, in general, non-trivial.

Population studies disagree on the choice of  $\alpha$ , primarily because the choice of  $\alpha$  strongly effects the formation rate of key astrophysical objects. High values maximize the formation rate of double neutron star binaries whereas low values maximize the formation rate of low-mass X-ray binaries. Generally, population synthesis studies of low-mass X-ray binaries have assumed  $\alpha$  values near -2.7 (Kalogera & Webbink 1998), whereas studies of double neutron star binaries tend to prefer a flat distribution with  $\alpha = 0$  (Belczynski et al. 2002). Resolving this ambiguity is important because the choice of this value can change formation rates of, for example, neutron star binaries by nearly a factor of 100 (Fryer et al. 1999)! This is the difference between advanced LIGO detecting 10 binary inspirals per year versus 1 inspiral in 10 years.

The second critical parameter is the distribution of orbital separations,  $f(r)$ . This distribution is often taken to be a power law between some inner and outer limits,  $r_{in}$  and  $r_{out}$ , such that  $f(\log r) \propto (\log r)^\beta$  where  $\beta > 0$  indicates a preference for large orbital separations and  $\beta < 0$  indicates a preference for small separations.

## 1.2. Observational Constraints on Mass Ratios

Observational studies of binaries have reached widely varying, even disparate, conclusions regarding these key parameters (reviewed in Abt (1983); Larson (2001)). Garmany et al. (1980) found  $\alpha = 0 - 1$  for a sample of 67 massive spectroscopic binaries, suggesting that the mass ratio distribution is either flat or peaked toward massive companions. Among B2–B5 primaries, Abt et al. (1990) report a secondary star mass distribution consistent with the Salpeter (1955) IMF, corresponding to  $\alpha \simeq -2.3$ . In a spectroscopic study of solar type field stars, (Duquennoy & Mayor 1991) conclude  $\alpha \leq -2$  for systems with  $q > 0.1$ , consistent with secondaries drawn from a field star IMF. Adaptive optics imaging surveys for companions of B and A stars in the Scorpius OB2 Association (Kouwenhoven 2006; Kouwenhoven et al. 2005; Shatsky & Tokovinin 2002), however, find the mass ratio distribution to be well-characterized by  $\alpha = -0.4 - -0.5$ . Fisher et al. (2005) report a flat ( $\alpha \sim 0$ ) distribution of mass ratios among single-lined spectroscopic binaries (SB1s) in the solar neighborhood, while double-lined spectroscopic binaries (SB2s) show a peak near  $q \sim 1$ .

Arguments abound over whether this  $q = 1$  peak is real or a selection effect arising from the fact that SB2s are only identified as such if the mass and luminosity ratios are near unity (Lucy & Ricco 1979; Halbwachs et al. 2003)

Several investigations have concluded that there are two populations of secondaries leading to a bimodal distribution of mass ratios. In summarizing data from the *Index Catalog of Visual Binary Stars* (Jeffers et al. 1963) Hogeveen (1990, 1992) and the 6th *Catalog of the Orbital Elements of Spectroscopic Binary Stars* (Batten et al. 1989) found that  $\alpha \leq -2$  for systems with mass ratios  $q > q_0$  where  $q_0 \simeq 0.3$ . This is roughly equivalent to secondary masses being drawn from the field star initial mass function (Salpeter 1955; Scalo 1986; Kroupa et al. 1991). For extreme mass ratio systems,  $q < 0.3$ , Hogeveen (1992) finds a flat distribution (i.e.,  $\alpha \simeq 0$ ). Furthermore, the turnover point,  $q_0$ , may vary inversely with primary mass, but the Hogeveen (1992) sample did not include O stars. Using radial velocity data of solar-type F7-K stars with periods  $P < 10$  yrs, Halbwachs et al. (2003) find a broad peak in the mass ratio distribution near  $q = 0.5$  and a sharp peak near  $q = 0.8$ . In a spectroscopic study of low-mass stars, Goldberg & Mazeh (1994) report a peak in the mass ratio distribution near  $q = 0.2$  and a smaller peak near  $q = 0.8$ . From a spectroscopic survey of eclipsing OB binaries in the *SMC* (Harries et al. 2003; Hilditch et al. 2005) Pinsonneault & Stanek (2006) conclude that massive primaries have two populations of companions: a “twin” population with  $M_2 > 0.95M_1$  comprising 45% of binaries, and a population drawn from a flat mass distribution ( $f(q) = \text{constant}$  corresponding to  $\alpha=0$ ) comprising 55%. This report echos earlier findings among low-mass stars that short-period ( $P < 40$  d) binaries have a “twin” component comprising 10% – 50% of the total population (Lucy & Ricco 1979; Tokovinin 2000). Lucy (2006) reassessed the Hogeveen (1992) study using data from the 9th *The Ninth Catalogue of Spectroscopic Binary Orbits* (Pourbaix et al. 2006) and concluded that the data support an excess of  $q \simeq 1$  “twin” systems.

### 1.3. Observational Constraints on Orbital Separations

Duquennoy & Mayor (1991) use a radial velocity survey of G dwarf primaries to conclude that the distribution of orbital periods for nearby binaries is broad and approximately Gaussian in  $\log P$  having  $\overline{\log P} = 4.8$  and  $\sigma_{\log P} = 2.3$  with  $P$  in days. Therefore, the distribution of orbital separations should be approximately log-normal as well, with a mean of  $\sim 25$  AU. This result contrasts with others that indicate the distribution of orbital separations is flat in log space,  $f(\log r) \propto (\log r)^0$ , corresponding to  $f(r) \propto (r)^{-1}$  (i.e., Öpik’s law; Öpik 1924). Kouwenhoven (2006) and Shatsky & Tokovinin (2002) measured separations  $r > 30$  AU for visual binaries in Sco OB2 and find a flat distribution consistent with Öpik’s

law. Lépine & Bongiorno (2007) report a flat distribution of separations among *Hipparcos* common proper motion stars in the solar neighborhood.

#### 1.4. Observational Constraints on Binary Fraction

Estimates for the binary fraction,  $F$ , among massive stars vary widely, and such estimates are always lower limits given that very close, very distant, and very low-mass companions are difficult to detect. Here, we use  $F$  to mean the fraction of all primary stars having exactly one secondary. We do not explicitly consider triple and higher order systems, even though Garcia & Mermilliod (2001) report that a significant fraction of massive close binaries may have multiplicity  $> 2$ . Abt (1983); Abt et al. (1990); Poveda et al. (1982) report binary fractions of at least  $F = 0.7$ , and suggest that the binary fraction may be close to 100% after corrections for incompleteness. Among O stars in clusters and associations, Gies (1987) report binary fractions of  $F = 26\% - 55\%$ . Mason et al. (1998) find binary fractions of at least  $F = 59\% - 75\%$  for O stars in clusters and associations. Garcia & Mermilliod (2001) tabulate multiplicity statistics for O stars in a variety of cluster environments, and they conclude that the binary fraction varies between  $F = 14\%$  and 80%, with denser clusters having lower binary fractions.

#### 1.5. Scope of this Paper

Despite a wealth of observational data on parameters of binary systems, there is little apparent agreement, leaving reasonable doubt as to whether the results are reconcilable. Much of the disagreement can be explained by observational and sample selection biases. Both spectroscopic radial velocity surveys and direct imaging surveys for companions of massive primaries become incomplete at low mass ratios below  $q \sim 0.25$ . Secondaries in close, extreme mass ratio systems with massive primaries are presently undetectable with either technique and are likely to remain so in the near future. Thus, estimates of  $F$ ,  $f(r)$ , and  $f(q)$  at low  $q$  must be made by extrapolating some functional form of the distribution based on data from systems with larger  $q$  and/or large  $r$ . Radial velocity surveys such as Garmany et al. (1980); Abt et al. (1990); Duquennoy & Mayor (1991); Halbwachs et al. (2003); Goldberg & Mazeh (1994); Harries et al. (2003); Fisher et al. (2005) preferentially detect close, short-period companions ( $a \leq \text{few} \times 10 \text{ AU}$ ) while imaging surveys such as Shatsky & Tokovinin (2002); Kouwenhoven et al. (2005); Kouwenhoven (2006); Lépine & Bongiorno (2007) preferentially detect more distant, long-period companions. If the fundamental parameters of binaries are different for close versus distant binaries (Abt et al. 1990; Mazeh et al. 1992; Mason et al.

1998), then the variety of reported results might be partially understood in terms of these observational selection effects (see Fig 1 of Mason et al. (1998); also Tout (1991)). Furthermore, many studies do not explicitly describe the limits,  $r_{in}$ ,  $r_{out}$  over which the results are valid, complicating comparisons between surveys.

The statistics on companions to massive stars are especially uncertain as there have been few studies of massive binaries since the survey of Garmany et al. (1980). For massive primary stars, the small number of broad spectral features, coupled with rotational broadening, make radial velocity measurements difficult, and the Garmany et al. (1980) sample may have missed binaries below velocities of  $50 \text{ km s}^{-1}$ . More than half of their sample consisted of double-lined spectroscopic binaries, thereby introducing a bias in favor of nearly equal mass components with large relative radial velocities. About half of the sample consisted of evolved O stars, selected on a magnitude-limited basis from throughout the sky. Given the selection biases and lack of a common origin and age for this sample, the conclusions of Garmany et al. (1980) may not apply to the general population of zero-age massive binaries. Similarly, the conclusions of Pinsonneault & Stanek (2006) are based upon a small number of eclipsing systems in the SMC, and are, therefore, most sensitive to systems of equal mass and radius so that no firm conclusions can be drawn (Lucy 2006).

In this paper, we analyze data from the radial velocity survey of 120 O and early-B stars in Cygnus OB2 (Kiminki et al. 2007) to help resolve these disparate conclusions regarding the binary characteristics of massive stars. The new data more than double the sample size of the Garmany et al. (1980) study, include massive stars down to early B spectral types, and often involve more epochs of observations. Although orbital parameters for a large number of systems are not yet available, we use the observed distribution of radial velocities, in conjunction with Monte Carlo models, to test several popular formulations of  $F$ ,  $f(q)$ , and  $f(r)$  from the literature (Pinsonneault & Stanek 2006; Hogeveen 1992; Garmany et al. 1980). Using only the raw velocities of a large sample of stars from one young OB association mitigates many of the selection and evolutionary effects responsible for conflicting results from more general binary surveys and catalogs (Tout 1991).

We find that we are able to constrain the probable values for  $\alpha$  and  $\beta$  to a narrow region of parameter space, subject to reasonable assumptions about the boundary conditions of the mass ratios and orbital separations. Only select combinations of  $\alpha$ ,  $\beta$ ,  $r_{in}$ ,  $r_{out}$ , and  $F$  can reproduce the levels of velocity variation seen in the data. Some canonical parameterizations for binary characteristics are inconsistent with the data and can be ruled out. Our immediate intent is to provide improved input parameters for population synthesis models that predict the rates of energetic phenomena in the Milky Way and at cosmic distances. We also expect that these results will have implications for the formation scenarios of massive stars which

are currently under debate (Bonnell et al. 1998; Wolfire & Cassinelli 1987; Krumholz et al. 2005).

## 2. The Data

Kiminki et al. (2007) report on a 6-year radial velocity survey of 120 early-type probable members of the Cygnus OB2 Association. Cygnus OB2 was chosen as a target for long term radial velocity study to determine the binary fraction and mass ratio distribution among massive binaries *in a populous young OB association where the stars are of comparable age and stellar evolutionary effects are minimized*. However, even in the  $\sim$ 2–3 Myr old Cygnus OB2, the presence of a variety of evolved stars suggests that the star formation process was non-coeval (Massey & Thompson 1990; Hanson 2003).

Spectroscopic observations from the Lick Observatory Shane telescope, the Keck Observatory Keck I telescope<sup>1</sup>, the Kitt Peak National Observatory<sup>2</sup> WIYN<sup>3</sup> telescope, and Wyoming Infrared Observatory 2.3 m telescope (WIRO) over the period 1999 July to 2005 October were used to measure radial velocity variations of stars earlier than spectral type B3. Sample stars were observed on at least 3 epochs over this period. Some stars have as many as 18 epochs of data. The mean and median number of epochs are 7.6 and 7.0 respectively. The time sampling is irregular, as imposed by telescope schedules and weather conditions. Sampling is additionally modulated by the observing season for Cygnus (June through November). The data were reduced and analyzed using cross-correlation techniques, as described by Kiminki et al. (2007).

Figure 1 shows the analytical two-body relationship between velocity semi-amplitude and orbital period for binary systems with a  $10 M_{\odot}$  primary. Solid lines indicate the loci of systems with equivalent mass ratios,  $q \equiv M_2/M_1 = 1.0, 0.1, 0.01$ . Dotted lines indicate loci of common orbital separations,  $r = 0.1, 1.0, 10 AU$ . The dark gray area in the upper-

---

<sup>1</sup>Some of the data presented herein were obtained at the W.M. Keck Observatory, which is operated as a scientific partnership among the California Institute of Technology, the University of California and the National Aeronautics and Space Administration. The Observatory was made possible by the generous financial support of the W.M. Keck Foundation.

<sup>2</sup>NOAO is the national center for ground-based nighttime astronomy in the United States and is operated by the Association of Universities for Research in Astronomy (AURA), Inc., under cooperative agreement with the National Science Foundation.

<sup>3</sup>The WIYN Observatory is a joint facility of the University of Wisconsin, Madison, Indiana University, Yale University, and the National Optical Astronomy Observatories.

right demarcates the prohibited region of parameter space where  $q \geq 1$ . The light gray area indicates the portion of parameter space sampled in this survey. The data are sensitive to primary velocity semi-amplitudes  $\geq 5 - 10 \text{ km s}^{-1}$ , periods shorter than  $\sim 2 \times 6$  years and orbital separations  $\leq \sim 2 \times 10 \text{ AU}$ .

The data presented in Kiminki et al. (2007) show at least several dozen stars with strong radial velocity variations at the level of  $> 20 \text{ km s}^{-1}$  and dozens of additional velocity-variable candidates with semi-amplitudes down to the survey sensitivity of  $\sim 5 - 10 \text{ km s}^{-1}$ . There are also  $\sim 6$  probable double-lined spectroscopic binaries, but the individual components are poorly resolved in most of our data, so these systems are, for present purposes, treated as single-lined binaries. For this analysis, we removed from the main sample of 120 objects (Table 5 of Kiminki et al. (2007)) six stars later than B4. The remaining sample used for analysis is 114 objects. These include the stars identified as probable members by Massey & Thompson (1990) plus additional early B type members identified photometrically by Massey & Thompson (1990) and classified by Kiminki et al. (2007). Given the significant uncertainties in the photometric distances, we have undoubtedly included a few foreground and background stars. The distribution of photometric distances (Figure 5 of Kiminki et al. (2007)) is nearly Gaussian with only a couple of outliers, suggesting that the sample does not suffer significant contamination from field stars. Including a few field objects in the 114-star sample will not measurably impact the conclusions, even if the binary characteristics of field OB stars are different than the Cygnus OB2 members.

Figure 2 plots the log of the assigned spectroscopic masses (Martins et al. 2005; Humphreys & McElroy 1984) for each primary star versus the quantity  $V_h \equiv 0.5|V_{max} - V_{min}|$ , where  $V_{max}$  and  $V_{min}$  are the maximum and minimum observed velocity for a given star.  $V_h$  is a measure of the velocity semi-amplitude of the primary, albeit an imperfect one because the velocity curves are not generally well sampled at all phases. We regard  $V_h$  as a lower limit on the true projected velocity semi-amplitude. Filled circles in Figure 2 denote main sequence OB stars while triangles denote evolved stars. The error bars show the mean uncertainty in the velocity measurements over all epochs for a given star. A small dispersion has been added to the masses in a few heavily populated mass bins to improve clarity. One O3If star (MT457 in the nomenclature of Massey & Thompson (1990)) at  $M = 80 M_\odot$  falls outside the maximum plot range. The typical velocity precision is  $\sim 5 - 15 \text{ km s}^{-1}$ , and it varies somewhat with source luminosity and observatory/instrument combination used. For example, the radial velocity uncertainties obtained with the WIYN telescope + Hydra spectrograph are often better than those obtained with the Lick 3 m telescope + Hamilton echelle spectrograph because of the higher signal to noise ratio achievable with the former. Kiminki et al. (2007) provide a more complete description of these data and place a lower limit on the binary fraction at 30% – 42%.

Figure 3 shows a histogram of the observed velocities and uncertainties. This Figure illustrates the distribution of velocity dispersions,  $V_{rms}$ , calculated from the multiple measurements of the 114 OB stars (solid line) along with the distribution of mean velocity uncertainties,  $\bar{\sigma}_v$  (dashed line). The dotted line shows the distribution of  $V_h$ . The lowest velocity bin from 0 to 5 km s<sup>-1</sup> is sparsely populated because observational errors scatter the data into higher velocity bins. The maximum observed semi-amplitudes fall mostly between 10 and 40 km s<sup>-1</sup>, with a significant tail toward higher velocities out to  $\sim$ 90 km s<sup>-1</sup>. The uncertainties lie in the characteristic range 5 – 15 km s<sup>-1</sup>.

For comparison, Figure 4 shows the distribution of properties for O-type systems from Garmany et al. (1980). The left panel shows a histogram of the velocity semi-amplitudes for the new observations of O stars presented in Table 3 and Figure 1 of Garmany et al. (1980). Note the differences compared to our Figure 3. Most striking in the Garmany et al. sample is the relative lack of stars in the velocity range 20–80 km s<sup>-1</sup> and the relative excess of stars in the range 80–120 km s<sup>-1</sup>. Significant selection affects may drive these differences. The Garmany et al. (1980) sample was magnitude limited and contained stars at a variety of evolutionary stages, including a large fraction of supergiants. For such systems, mass exchange and transfer of angular momentum between orbital and rotational components may have altered the original binary mass ratios and separations. Therefore, the Garmany et al. (1980) sample may not be representative of the general population of massive binaries at zero age. The middle panel of Figure 4 is a histogram of mass ratios,  $q$ , for the O type binaries from Table 3 of Garmany et al. (1980).<sup>4</sup> The histogram shows a preference for mass ratios near unity and is consistent with a flat ( $\alpha = 0$ ) or rising distribution ( $\alpha > 0$ ) with increasing mass ratio. The right panel of Figure 4 shows a derived semi-major axis distribution for the O type binary systems from Table 3 of Garmany et al. (1980) assuming an average orbital inclination of 60°. The dashed line is a best fit Gaussian curve which peaks near  $\log(r) = -0.8$  or  $\sim 0.15$  AU. This panel shows that the O-type binaries from Garmany et al. are preferentially those with small orbital separations, as might be expected since these are the easiest to detect. Garmany et al. (1980) did consider whether the lack of systems with small velocity amplitudes implied a true absence of such systems or a merely limitation on their detection. They concluded that such low-amplitude systems should have been detected as part of their survey and that the preference for equal mass components was a real effect.

---

<sup>4</sup>Here, we have included only the stars with new observations denoted by an asterisk in their Table 3.

### 3. Modeling Binary Characteristics

#### 3.1. Monte Carlo Modeling of Radial Velocities

We wrote a Monte Carlo code to simulate the radial velocity variations expected for Cyg OB2 primaries based upon analytic prescriptions of binary mass ratios and orbital separations. We initially assumed a binary fraction of  $F = 1.0$  so that every primary star has one companion. Statistically, this means that single stars are treated as systems with very low mass companions, very large separations, or very low inclinations. However, this is a useful approach to obtain an initial lower limit on  $\alpha$ . For each of the 114 primary stars (Kiminki et al. 2007) of mass  $M_1$  and observed velocity variations characterized by  $V_h$  and  $V_{rms}$ , the Monte-Carlo code randomly assign a secondary star of mass  $M_2$  based upon a distribution of mass ratios,  $f(q)$  where  $q \equiv M_2/M_1$ . The mass ratios are drawn from a population described by  $f(q) \propto q^\alpha$  where  $\alpha$  is the power-law index of the mass ratio distribution over the range  $q_{low} < q < 1$ . Initially, we adopt  $q_{low} = 0.02$  so that the lowest mass secondaries for our least-massive  $\sim 8 M_\odot$  primaries are  $0.16 M_\odot$  and  $\sim 1 M_\odot$  for the handful of very massive  $50 M_\odot$  stars. Such masses are sufficiently low that the secondaries produce negligible radial reflex motion in their primaries—well below the velocity sensitivity of the data. We consider values of  $\alpha$  between -3.0 and 2.0.  $\alpha > 0$  describes a secondary star mass distribution peaked toward the primary mass.  $\alpha = 0$  corresponds to a flat distribution of secondary masses. The Monte-Carlo code assigns an orbital separation,  $r$ , drawn from a distribution described by  $f[\log(r)] \propto [\log(r/r_{in})]^\beta$  with  $r_{in} < r < r_{out}$  and  $r$  in A.U. Öpik's Law ( $\beta = 0$ ) corresponds to a parent population of orbital separations uniformly distributed in  $\log(r)$  between  $\log(r_{in})$  and  $\log(r_{out})$ .  $\beta = \pm 3$  corresponds to distributions peaked toward large/small separations, respectively.

Because the power-law slope,  $\beta$ , that best describes the orbital separations of the data will depend upon the chosen boundaries,  $r_{in}$  and  $r_{out}$ , we explore a small 3x3 grid of values:  $r_{in} = 0.020, 0.063, \& 0.200 AU$  and  $r_{out} = 100, 1000, \& 10000 AU$ . These inner limits correspond to 4.2, 13, and 43  $R_\odot$ . For a main-sequence B0 star, representative of our targets, these inner limits correspond to 0.56, 1.7, and 5.8  $R_*$ . Thereby, the smallest two values for  $r_{in}$  are firm lower limits, representing separations where significant mass transfer and common envelope evolution would take place. Although these values are physically implausible in general, we include them to illustrate the sensitivity of the simulations to this parameter. The third value, 0.20 AU, is the largest reasonable choice for  $r_{in}$ , as it is larger than several of the orbital separations for short-period Cyg OB2 binaries reported in Kiminki et al. (2007) and Garmany et al. (1980) ( $\sim 0.15 AU$ ). The minimum adopted outer limit,  $r_{out} = 100 AU$  is small compared to observed orbital separations in wide binaries which may extend to several thousand AU (e.g., Kouwenhoven et al. 2005; Duquennoy & Mayor 1991). The maximum

adopted outer limit,  $r_{out} = 10000 \text{ AU}$ , is sufficiently large that few systems are likely to remain bound at such distances, especially in the dense stellar environments where OB stars are born. Lépine & Bongiorno (2007) report that among nearby *Hipparchos* binaries, the Öpik’s Law distribution of separations fits the data out to a maximum of  $r = 4000 \text{ AU}$ , beyond which the number of companions drops, consistent with gravitational disruption.

In the interest of minimizing free parameters, we assume that the orbits have zero eccentricity. The resulting period and velocity semi-amplitude of the simulated binary system is computed  $N_{iter}$  times, where  $N_{iter}$  is typically 100 Monte-Carlo iterations. For each simulated system, the velocity curve is sampled at a random phase angle  $N_{obs}$  times, where  $3 < N_{obs} < 18$ , the actual number of observations of a given star. The code assigns a random inclination angle,  $i$ , for each system, where  $i$  is generated by allowing the angular momentum vector of the simulated system to lie anywhere on a sphere. The mean observational velocity uncertainty for each individual star, normally distributed about zero, is then added to the simulated velocity. As a test, we also performed simulations using the actual uncertainties for each measurement of each star and we found that the results differed insignificantly from using the average uncertainty.

For each Monte Carlo run with a given pair of  $\alpha$  and  $\beta$ , the *simulated* distribution of  $V_h$  and  $V_{rms}$  for 114 stars is compared to the *observed* distribution using a two-sided K-S test. The probabilities that the *simulated* and *observed* distributions of  $V_h$  and  $V_{rms}$  ( $P(V_h)$  and  $P(V_{rms})$ , respectively) are drawn from the same population are averaged over 100 Monte Carlo iterations and tabulated for later analysis. We found that both velocity metrics,  $V_h$  and  $V_{rms}$ , yield similar results and provide similar probabilistic constraints on the binary characteristics. While  $V_h$  is a better measure of the true semi-amplitude, it is also less robust than  $V_{rms}$  against outliers or measurements with large uncertainties. Therefore, in subsequent discussion and figures we use the average probability,  $P_a$ , obtained from the arithmetic mean of  $P(V_h)$  and  $P(V_{rms})$ .

In Section 4 we will discuss the constraints imposed by this modeling approach. The Figures and discussion will show that there is degeneracy between  $\alpha$  and  $\beta$ —in general, large  $\alpha$  coupled with large  $\beta$  reproduce the velocity data approximately as well as small  $\alpha$  coupled with small  $\beta$ . Additional constraints are needed. One such constraint we consider is that Öpik’s Law ( $\beta = 0$ ) obtains. Another is the fraction of type Ib/c supernovae predicted by each model.

### 3.2. Monte Carlo Modeling of Type Ib/c Supernova Rates

The massive binary population can also be constrained by observations of energetic phenomena that arise from massive binary progenitors. A well-studied example is the fraction of core-collapse supernovae that occur in stars that have lost their hydrogen envelopes—type Ib/c supernovae. Podsiadlowski (1992) argued that most Ib/c supernovae are produced in binary star systems where mass transfer removes most/all of the hydrogen envelope, unveiling a type Ib/c supernova progenitor. Podsiadlowski (1992) assumed that 37% of binaries were close binaries that would undergo some mass transfer.

The fraction of type Ib/c supernovae predicted by population synthesis models must agree with observations *and* must self-consistently produce the levels of velocity variation seen in massive primaries, such as those in Cyg OB2. The fraction of type Ib/c supernovae relative to all core-collapse supernovae is  $f_{Ib/c} \equiv N_{Ib/c}/(N_{Ib/c} + N_{II})$ . Cappellaro et al. (1999) and Mannucci et al. (2005) give the observed fraction of type Ib/c supernovae in Sbc/d spiral galaxies such as the Milky Way as 15%. The more recent works of Li et al. (2007) and Leaman et al. (2007) revise this estimate upward to  $30\% \pm 11\%$ . Using binary population synthesis calculations, we can apply these fractions to further constrain the parameter space in our study. Any part of parameter space that produces a fraction of type Ib/c supernovae inconsistent with the observed fraction can be ruled out.

We used the binary synthesis code developed by Fryer et al. (1998, 1999) to calculate the total core-collapse supernova rate and the number of type Ib/c (stars that have lost their hydrogen envelopes at collapse) supernovae. Like Podsiadlowski (1992), we find that the primary formation path for type Ib/c supernovae begins with a close binary where the more massive primary envelops its companion in a common envelope phase. The companion spirals into the envelope of the massive primary, ejecting the hydrogen envelope. After the common envelope phase, the primary will continue to lose mass in a wind. For this paper, we will assume any star that loses its entire hydrogen envelope has the potential to become a type Ib/c supernova. Because mass is lost in winds as well, even systems (especially those at high metallicity) that merge in the common envelope phase without ejecting the hydrogen envelope can make type Ib/c supernovae. Systems with more extreme mass ratios (i.e.,  $q \leq 0.2$ ) are more likely to go through a common envelope phase and systems with such low-mass companions dominate the formation rate of type Ib/c supernovae. Figure 5 shows the range of primary masses and orbital separations that form Ib/c supernovae for 4 separate values of the system mass ratio. As  $q$  increases, the system tends to undergo more stable mass transfer without a common envelope phase. Most of these systems do not become type Ib/c supernovae. These simulations are based on our standard wind assumptions in which wind mass loss rates are set to 10% of the Woosley et al. (1995) values. Beyond  $32 M_{\odot}$ , these

primary star winds will also produce type Ib/c progenitors, regardless of companion mass. However, this corresponds to only a small fraction of our type Ib/c supernova rate.

The other requirement for a star to produce a type Ib/c supernova is that it actually explode as a supernova. We assume any primary with an initial mass above  $9 M_{\odot}$  will produce a supernova. Although the total rate of type Ib/c supernova does depend on this choice, the dependence on the type II rate is nearly identical and varying this value in the  $8 - 10 M_{\odot}$  range leads to variations in the rate of 2-3% for the bulk of our parameter study. We also assume that stars that have helium cores in excess of  $11 M_{\odot}$  collapse directly to black holes and don't form supernovae. Varying this value of the helium core mass over the  $8 - 15 M_{\odot}$  range yields variations in the rate of less than 1%. This is not surprising because the number of such high-mass systems is quite small.

In this paper, we focus our binary population synthesis studies on the mass distributions of the stellar components and the orbital separation. These distributions are varied according to range of parameters studied in the analysis of our observations and constitute over 10,000 different population synthesis calculations each including 100,000 binaries for each calculation. In all of these calculations, we assume the eccentricity is zero. If we instead assume the eccentricity follows a flat distribution between 0 and 0.8, we can increase the rate by 5%.

We have already discussed the dependence of our ratios on some of the many free parameters in population synthesis: e.g. critical mass for supernova formation. Let's briefly discuss some of the remaining free parameters. We assume a single Maxwellian kick distribution with a mean value of  $300 \text{ km s}^{-1}$ . Because nearly all of the type Ib/c supernovae are formed in hydrogen envelope stripping in the common envelope inspiral of the companion star into the massive primary, the rate does not depend strongly on the choice of this kick. We have varied the value of this mean value from  $100 \text{ km s}^{-1}$  to  $600 \text{ km s}^{-1}$  as well as using the bimodal kick distribution of Fryer et al. (1998) and the rate does not change by more than 5%. For mass transfer, we use the same formalism as Fryer et al. (1999) with mass transfer parameters  $\alpha_{\text{MT}} = 1.0$  and  $\beta_{\text{MT}} = 0.5$  and a common envelope efficiency  $\alpha_{\text{CE}} = 0.5$ . Varying these values for a wide range of values (e.g.  $0.2 < \alpha_{\text{CE}} < 1.0$ ) yields variations in the ratio of 10-30%.

The final two uncertainties studied in our calculations are our assumed stellar radii and stellar mass loss rates. Here again, we use the standard Fryer et al. (1998) values. But if we allow a factor of 2 variation (both increase and decrease) in these values, the ratio of type Ib/c supernovae to type II supernovae can vary by nearly 50%. Uncertainty is one of the dominant uncertainties in the population synthesis of binary systems: the error in the stellar radius. If the stellar radii are smaller, we produce fewer common envelope systems with a

larger fraction of the remaining common envelope systems leading to mergers prior to the ejection of the hydrogen envelope. This error dominates our 50% error. Clearly we can vary the population synthesis parameters to make many of the models fit to the data. But if we assume we know the stellar radii and take standard values for common envelope efficiencies, our calculation errors can be limited to 5–10% effects, allowing us to place strong constraints on the assumed distributions of initial masses and separations.

## 4. Results of Modeling

### 4.1. Binary Characteristics for single power-law distributions of $q$ and $r$

Panels within Figure 6 show probability contours (solid lines) depicting the likelihood,  $P_a$ , that a given combination of  $\alpha$  and  $\beta$  reproduces the distribution of velocities in the data for a minimum mass ratio of  $q = 0.02$  and binary fraction of  $F = 1.0$ . The 3x3 grid corresponds to  $r_{in} = 0.020 \text{ AU}$  (left column),  $r_{in} = 0.063 \text{ AU}$  (middle column),  $r_{in} = 0.200 \text{ AU}$  (right column), and  $r_{out} = 10000 \text{ AU}$  (upper row),  $r_{out} = 1000 \text{ AU}$  (middle row),  $r_{out} = 100 \text{ AU}$  (lower row). The horizontal line in each panel marks the nominal  $\beta = 0$  (Öpik’s Law) distribution of separations. The dotted contours in each panel depict the predicted fraction of type Ib/c supernovae in our Monte Carlo models. These contours run from 10% to 40% in increments of 5%.

The panels in Figure 6 demonstrate the sensitivity of the best-fitting solutions for  $\alpha$  and  $\beta$  to the adopted  $r_{in}$  and  $r_{out}$ . Each panel contains a crescent-shaped ridge of highest likelihood contours ( $P_a \geq 50\%$ ). Values outside of this region drop to probabilities  $< 10\%$  over much of the plotted parameter space. These contours show that the best-fitting  $\alpha$  and  $\beta$  are correlated—larger orbital separations are required (i.e., larger  $\beta$ ) when mass ratios are peaked toward unity, while smaller orbital separations are required for mass ratio distributions with secondaries drawn from a field star IMF. The ridge of peak likelihood separates parameter space into two regimes: to the left of the ridge of solid contours the models fail to produce enough high-velocity systems and are inconsistent with the data; to the right of the peak contour ridge, the models produce too many high-velocity systems relative to the data.

For a flat distribution of orbital separations described by Öpik’s law, the best-fitting values for  $\alpha$  lie in the broad range  $-1.2 < \alpha < 1.0$  depending on the choice of radial limits. For the most reasonable choices  $r_{in} = 0.063\text{--}0.200 \text{ AU}$  and  $r_{out} = 1000 \text{ AU}$ ,  $\alpha$  lies in the range  $-0.6 - 0.0$ , broadly consistent with observational estimates of (Kouwenhoven et al. 2005; Kouwenhoven 2006; Garmann et al. 1980). The dashed contours depicting  $f_{Ib/c} = 0.25\text{--}0.35$

intersect the  $\beta = 0$  line and the solid contour ridge, indicating a Ib/c fraction about twice the older observational estimates of 15% (Mannucci et al. 2005; Cappellaro et al. 1999) but consistent with the most recent determinations of  $30\% \pm 11\%$  (Li et al. 2007; Leaman et al. 2007). Ib/c fractions of  $f_{Ib/c} < 0.20$  are inconsistent with the data in all panels except the upper-right which shows the (perhaps unrealistically) large radial limits of  $r_{in} = 0.20$  AU and  $r_{out} = 10,000$  AU. It is noteworthy that, in all of the panels, mass ratio distributions described by  $\alpha < -2$  are unlikely (contours levels  $< 30\%$ ) even if the distribution of orbital separations favors close companions (small  $\beta$ ). Furthermore, any  $\alpha < -1$  for the most plausible radial limits in the middle or upper middle panels would require  $f_{Ib/c} > 0.40$  and  $\beta < -0.3$ , in disagreement with observational results.

Figure 7 shows the distribution of observed and simulated velocity semi-amplitudes,  $V_h$ , (solid and dashed lines, respectively) for a subset of models that produce  $P_a \simeq 60\%$  from the contour ridge in the middle-right panel of Figure 6. The left panel of Figure 7 shows a simulation with  $\alpha = 0.4$ ,  $\beta = 0.10$ , and the right panel shows  $\alpha = -0.6$ ,  $\beta = -0.20$ . Each panel is labeled with the probability that the two histograms are drawn from the same parent population. Both combinations of  $\alpha$ ,  $\beta$  yield probabilities of  $P(V_h) \simeq 0.60$  and lie along the ridge line of peak likelihood. There is good agreement between the data and simulations based on the two-sided K-S “D” statistic which quantifies the maximum difference between the cumulative distribution functions of the two data sets. An analysis of the cumulative distribution functions shows that, for these best-fitting models, the maximum differences occur in the range  $10\text{--}40$  km s $^{-1}$  and  $80\text{--}100$  km s $^{-1}$  in roughly equal proportion. This means that, in some Monte Carlo iterations, differences in the high-amplitude tail of the velocity distributions limit the agreement between the models and data; in other iterations, the models fail to produce the observed velocity distribution on the low-amplitude side of the histogram. The lack of systematic trends in the velocity at which the K-S “D” maximum occurs may be taken as an indication that the comparison is limited by sample size and measurement uncertainties. If, for example, the K-S “D” maximum difference always occurred at small  $V_h$  amplitudes, we would suspect a systematic problem with the adopted velocity uncertainties which are responsible for the objects in the lowest velocity bins. If, on the other hand, the K-S “D” maximum difference always occurred at large  $V_h$  amplitudes, we might suspect the presence of a second population of close binaries which was responsible for the large-amplitude systems. We will return to this latter possibility in a subsequent section.

Figure 8 shows contour plot comparisons of the data with Monte Carlo simulations in the same manner as Figure 6, except for a binary fraction of  $F = 0.8$ . The overall level of agreement between the models and the data is lower in each panel by  $\sim 10\%$  when compared with the corresponding panel of Figure 6. The contours are qualitatively similar

to those in Figure 6 in that the ridge of peak likelihood reaches  $P_a \sim 50\%$  in most panels, but it is shifted slightly toward larger  $\alpha$  and smaller  $\beta$ . Variations between panels once again highlight the sensitivity of the best-fitting solutions to the adopted radial boundary conditions. For instance, the middle-right panel ( $r_{in} = 0.20$ ,  $r_{out} = 1000$ ) shows a peak likelihood of  $P_a > 60\%$  for an Öpik's Law distribution of  $r$ , but only for  $\alpha > 0.5$ , meaning that mass ratios must be peaked toward unity. This is because, with fewer binaries, the observed levels of velocity variation can only be reproduced with larger mass ratios and/or smaller separations. Thus, the Garmany et al. (1980) mass ratio distribution peaked toward unity can be consistent with the data, but only if the binary fraction is  $F < 0.8$  and only for somewhat large values of  $r_{in} = 0.20$  AU, i.e., larger than many of the systems observed by Garmany et al. (1980). For the most plausible radial limits ( $r_{in} = 0.063$ ,  $r_{out} = 1000$ ) in the center panel, the most probable value for  $\alpha$  is  $\sim 0.0$  for  $\beta = 0$ . This implies  $f_{Ib/c} = 0.20 - 0.25$ , at the lower end of current observational constraints (Li et al. 2007; Leaman et al. 2007). Any of the other panels for plausible radial limits (upper-middle or middle-right panels) require  $f_{Ib/c} < 0.20$ , a value that is increasingly inconsistent with observational limits.

Figure 9 shows contour plot comparisons of the data with Monte Carlo simulations in the same manner as Figure 6 for binary fractions of  $F = 0.6$ . Compared with the corresponding panels of Figure 8, the solid contours in each panel shows lower levels of agreement between models and data by about 10%. This is especially true in the middle and upper-middle panels which represent the most plausible radial boundary limits ( $r_{in} = 0.063 - 0.200$ ,  $r_{out} = 1000 - 10000$ ). These panels also show that mass ratio distributions with  $\alpha < -2$  are highly inconsistent with the data even if the orbital separations are preferentially very small ( $\beta < -1$ ) and  $r_{in} = 0.020$  AU. Thereby, the field IMF distribution for secondary star masses is highly improbable given that  $r_{in} = 0.020$  would require many systems in common envelopes even for main-sequence primaries. Reasonable agreement with the data ( $P_a > 50\%$ ) is only achievable with  $\alpha > 0$  and with  $r_{out} = 100$  AU (lower row). Because  $r_{out} = 100$  AU is implausible (no long-period companions!) and any of the panels for the most probable radial limits (middle or upper-middle) require  $f_{Ib/c} < 0.15$ , at odds with current estimates (Li et al. 2007; Leaman et al. 2007), we conclude that Figure 9 contains no acceptable portion of parameter space where a good fit between the models and data can be achieved. A binary fraction as of  $F = 0.6$  or lower is highly improbable in Cyg OB2.

In summary, the sequence of Figures 6, 8, 9 shows the degeneracies between  $\alpha$  and  $\beta$  and the sensitivity of the best-fitting solutions to the adopted boundaries of the power-law parameterization of separations,  $f(r)$ . Distributions of  $q$  favoring extreme mass ratios  $\alpha < -2$  universally require very small separations ( $\beta < -1$ ) in disagreement with observations supporting the canonical flat Öpik's Law distribution. For plausible inner and outer boundaries, the most probable values for  $\alpha$  lies in the range  $-0.6 - 0.0$  for  $F = 1.0$  and  $0.0 -$

1.0 for  $F = 0.8$ . Binary fraction  $F < 0.8$  would imply low fractions of type Ib/c supernovae,  $f_{Ib/c} < 0.20$ , inconsistent with current estimates.

#### 4.2. Comparison with the Hogeveen Distribution of $q$

Hogeveen (1990, 1992) proposed that  $f(q) \propto q^{-2.0} - -2.7$  for  $q > q_0$  where  $q_0 = 0.3$  for B star primaries, and  $f(q) \propto q^0$  (i.e., flat) for  $q < q_0$ . The relative numbers of systems above and below  $q_0$  is not given. We used an adapted Monte Carlo code to perform comparisons between the data and the predictions of the Hogeveen (1992) mass ratio distribution. We adopted a two-component power-law distribution of  $q$  with variable normalization for each component so that they yield the same  $f(q)$  at  $q_0$ . The component with  $q < q_0$  has fixed  $\alpha(q < q_0) = 0$  while  $\alpha(q > q_0)$  is allowed to vary freely. This effectively means that the fraction of systems with  $q > q_0$  varies with  $\alpha$ . For  $\alpha = 2.0$ , 90% of systems have  $q > q_0$ ; for  $\alpha = 0.0$ , 70% of systems have  $q > q_0$ ; for  $\alpha = -2.0$ , 48% of systems have  $q > q_0$ . We compared the velocity distribution of the data to the expectations of Monte Carlo simulations in the same manner as for the simple power-law parameterizations of  $f(q)$  and  $f(r)$  above. We note that in the limiting case  $\alpha(q > q_0) = 0$ , the predictions of the Hogeveen (1992) mass ratio distribution and the power-law formulation discussed above are identical, within the noise of the Monte Carlo procedure employed.

Figure 10 shows probability contour plots as a function of  $\alpha(q > q_0)$  and  $\beta$  for a range of  $r_{in}$  and  $r_{out}$  as in Figure 6. The ridge of peak likelihood exceeds 60% in some panels. In particular, the center ( $r_{in} = 0.063$ ) and middle-right ( $r_{in} = 0.20$ ) panels show best agreement with the data. Both panels have  $r_{out} = 1000$  AU. The center panel shows that for the nominal Öpik's Law distribution of separations, the most probable values for  $\alpha$  lie in the range  $-3.0 < \alpha < -2.0$ , consistent with the Hogeveen formulation for  $q > q_0$ . However, the predicted fraction of type Ib/c supernovae is  $f_{Ib/c} = 0.35 - 0.40$ , at the upper edge of current estimates (Li et al. 2007; Leaman et al. 2007). In most other panels,  $\alpha < -2$  is inconsistent with the data. The middle-right panel shows that for the Öpik's Law distribution of separations, the most probable values for  $\alpha$  lie in the range  $-1.0 < \alpha < 0.0$ . Hence, the most probable value for  $\alpha$  for the Hogeveen mass ratio distribution is much more sensitive to the choice of  $r_{in}$  than for the simple power-law distribution of  $q$ . This is because the peak contour ridge in each panel is nearly horizontal, a consequence of the fact that the actual distribution of mass ratios over the whole range  $q = 0.02 - 1$  varies comparatively little because the portion with  $q < q_0$  is unchanging. Under the Hogeveen formulation, the two-component power law with  $\alpha(q < q_0) = 0$  and  $\alpha(q > q_0) = -2$  essentially mimics a single power-law of intermediate slope,  $\alpha \simeq -0.6$ . The predicted fractions of type Ib/c supernovae

in the middle and middle-right panels are  $f_{Ib/c} = 0.35\text{--}0.40$  and  $f_{Ib/c} \simeq 0.30$  respectively.

Figure 11 shows probability contour plots as a function of  $\alpha$  and  $\beta$  for a range of  $r_{in}$  and  $r_{out}$  as in Figure 10, except for a binary fraction of  $F = 0.8$ . The overall level of agreement between the models and the data is lower in each panel by  $\sim 10\%$  when compared with the corresponding panel of Figure 10. The contours of peak likelihood are shifted toward larger  $\alpha$  and smaller  $\beta$  relative to Figure 10. In the center panel, the peak probabilities exceed 50%, and for an Öpik’s Law distribution of separations, the best fitting value of  $\alpha$  lies in the range  $-1 < \alpha < 0.3$ , inconsistent with the Hogeveen (1992) value of  $\alpha = -2$ . In the middle-right panel, the peak probabilities exceed 60%, but Öpik’s Law would require  $\alpha > 0.8$ . The predicted fraction of type Ib/c supernovae is  $f_{Ib/c} = 0.20\text{--}0.25$ , at the lower end of current estimates. The lower-middle panel shows probabilities exceeding 60% for Öpik’s Law and  $\alpha \simeq -2$ . However, this requires  $r_{out} = 100 \text{ AU}$ , and we argue previously that such a small outer bound on companion separations is not supported by observations. In summary, the Hogeveen (1992) mass ratios distribution and a binary fraction of  $F = 0.8$  produces slightly poorer overall agreement with the data. The best fitting models consistent with Öpik’s Law require  $-1 < \alpha < 1$  and  $r_{in} = 0.063\text{--}0.200$  and  $r_{out} \sim 1000 \text{ AU}$ . Simulations with  $F \leq 0.6$  show comparatively poor agreement with the data, similar to Figure 9, and would require  $f_{Ib/c} < 0.15$ , a value inconsistent with current measurements.

### 4.3. Comparison with a “Twin” Component Model Distribution of $q$

Given ample evidence in the literature for a significant “twin” population among short-period binaries (Pinsonneault & Stanek 2006; Tokovinin 2000; Lucy & Ricco 1979; Lucy 2006), we used a modified Monte Carlo code to simulate the expected velocity amplitudes from a two-component  $q$  distribution. The dominant component has a power-law distribution,  $f(q) \propto q^\alpha$  and  $f(\log r) \propto [\log(r/r_{in})]^\beta$  between the limits  $r_{in} = 0.063 \text{ AU}$  and  $r_{out} = 1000 \text{ AU}$ , with  $\alpha$  and  $\beta$  being free parameters, as described previously. The twin component comprises a fraction,  $T_{frac}$ , of the systems. We explore a range of twin fractions,  $T_{frac} = 0.40$ , 0.25, and 0.10. Allowing for the possibility that  $F$  may be less than unity, we define  $T_{frac}$  to be the fraction of systems with  $q \simeq 1$  *among those that are binary systems*. Motivated by observations that “twin” systems have small separations, presumably because they form within a causally connected region, we adopt a log-normal distribution with mean separation,  $\langle r_{Twin} \rangle$ , and Gaussian width,  $\sigma_{\log r}$ . We explore a range of typical separations,  $\langle r_{Twin} \rangle = 1.0$ , 3.9, and 15 AU (i.e.,  $\langle \log r_{Twin} \rangle = 0.0$ , 0.6, and 1.2). The smallest of these mean separations,  $\langle r_{Twin} \rangle = 1 \text{ AU}$ , is representative of the orbital distances required to produce OB star twins with orbital periods in the range few–60 days like the samples used

by (Pinsonneault & Stanek 2006; Tokovinin 2000; Lucy & Ricco 1979) to infer the presence of a twin population. We adopt  $\sigma_{\log r} = 0.6$  for the width of the twin population’s orbital separation distribution. (Exploration of larger and smaller values for  $\sigma_{\log r}$  yielded poorer levels of agreement with the data and we do not show these results in the interest of brevity.) The mass ratios for the twin component are uniformly distributed between  $q = 0.95\text{--}1.0$ . The lower mass limit for the power-law component described by  $f(q) \propto q^\alpha$  is  $q_{low} = 0.02$ .

Figure 12 shows a 3x3 grid of contour probability plots  $T_{frac}=0.40$  (left column),  $T_{frac}=0.25$  (middle column),  $T_{frac}=0.10$  (right column), and  $\langle r_{Twin} \rangle = 15 \text{ AU}$  (upper row),  $\langle r_{Twin} \rangle = 3.9 \text{ AU}$  (middle row),  $\langle r_{Twin} \rangle = 1.0 \text{ AU}$  (lower row). The horizontal line in each panel denotes Öpik’s Law ( $\beta = 0$ ). The panels in the right column having  $T_{frac} = 0.10$  closely resembles the center panel of Figure 6 where no twin component is included, indicating that twin fractions of  $<10\%$  do not measurably alter the results. In general, the lower row with  $\langle r_{Twin} \rangle = 1.0 \text{ AU}$  shows relatively poor agreement with the data—small mean separations yield too many large-amplitude systems. The peak probabilities exceed 60% in several panels, most significantly in the middle panel corresponding to  $\langle r_{Twin} \rangle = 3.9 \text{ AU}$ ,  $T_{frac}=0.25$  and in the middle-left panel corresponding to  $\langle r_{Twin} \rangle = 3.9 \text{ AU}$ ,  $T_{frac}=0.40$ . In these panels Öpik’s Law specifies best-fitting values for  $\alpha$  in the range  $-3.0 < \alpha < -1.3$ . The predicted fractions of type Ib/c supernovae are large in both cases, exceeding 0.40. In the middle-left panel showing  $\langle r_{Twin} \rangle = 3.9 \text{ AU}$ ,  $T_{frac} = 0.40$ , there is a broad region where the peak probabilities exceed 60% and reach 70%. In this case, if Öpik’s Law obtains, then  $\alpha < -2$ , consistent with the expectations of randomly pairing secondaries from the field IMF with massive primaries. Figure 12 illustrates that two-component  $q$  prescription of Pinsonneault & Stanek (2006) (45% of systems with  $q > 0.95$ , the remainder with  $\alpha = 0$ ) is not consistent with the data unless  $\beta > 0.5$ . That is, the probability of  $\alpha = 0$ ,  $\beta = 0$  is  $< 30\%$  for all of the panels. The presence of any significant twin component appears to require  $\alpha \leq -1$ .

Figure 13 shows a 3x3 grid of contour probability plots similar to Figure 12, but for a binary fraction of  $F = 0.8$ . The peak contours once again exceed 60%, primarily in the upper two rows of panels. The ridge of peak likelihood is shifted toward larger  $\alpha$  and smaller  $\beta$  relative to Figure 12. In most panels, the region with  $P_a > 0.60$  is smaller than in the corresponding panels of Figure 12, indicating slightly poorer overall agreement with the data. For an Öpik’s Law distribution of separations, the most probable values for  $\alpha$  lie in the range  $-1.5 - 0.0$  for twin fractions  $T_{frac} = 0.25\text{--}0.40$  and  $\langle r_{Twin} \rangle = 3.9\text{--}15 \text{ AU}$ . Models with  $\langle r_{Twin} \rangle = 1 \text{ AU}$  produce generally poorer agreement with the data, having peak likelihood  $< 50\%$ . The two-component  $q$  prescription of Pinsonneault & Stanek (2006) (45% of systems with  $q > 0.95$ , the remainder with  $\alpha = 0$ ) is not consistent with the data unless  $\langle r_{Twin} \rangle \simeq 15 \text{ AU}$ . At such large distances, OB star twins would have much longer

periods ( $\sim 10$  yr) than the  $\sim 30$ -day systems used to infer the presence of a twin population (Pinsonneault & Stanek 2006; Tokovinin 2000; Garmann et al. 1980). For  $\beta = 0$  and in panels with  $P_a \geq 0.60$  (middle, middle-left and upper-left), the predicted fractions of type Ib/c supernovae are  $f_{Ib/c} = 0.20\text{--}0.30$ , in broad agreement with observations (Li et al. 2007; Leaman et al. 2007).

Figure 14 shows a 3x3 grid of contour probability plots similar to Figure 12, but for a binary fraction of  $F = 0.6$ . The ridge of peak likelihood is now shifted ever farther toward large  $\alpha$ , and the peak probabilities do not much exceed 50% in most panels, indicating poorer agreement with the data compared to Figure 13. In those panels (middle, middle-left, upper-middle), Öpik’s Law would require  $\alpha > 0$ , in disagreement with the Pinsonneault & Stanek (2006) and field-star IMF distribution. Furthermore, the type Ib/c supernova fraction is  $f_{Ib/c} < 0.20$ , in disagreement with observations. Binary fractions  $F \leq 0.6$  appear improbable.

#### 4.4. Comparison with a Miller-Scalo Secondary Mass Distribution

Power-law parameterizations of the stellar initial mass function are appropriate only over a selected mass range. More realistic descriptions of the IMF include multiple power-law components with slopes that flatten toward lower masses (e.g., Miller & Scalo 1979; Scalo 1986; Kroupa et al. 1993). We used a modified Monte Carlo code to simulate the velocity distribution expected if the secondary masses were drawn from a distribution described by Miller & Scalo (1979) as parameterized in Equation 5 of Eggleton et al. (1989).

Figure 15 shows a 3x3 grid of contour probability plots similar to Figure 6 except that the ordinate in each panel is  $M_{low}$ , the lower mass limit at which the Miller & Scalo (1979) IMF is truncated. The columns and rows of panels show a range of  $r_{in}$  and  $r_{out}$ , labeled in each panel, as in Figure 6. The peak probabilities marginally exceed 60% in four panels: middle-left, center, upper-middle, and upper-right. Type Ib/c supernova fractions  $f_{Ib/c} = 0.20\text{--}0.40$  are broadly consistent with the data. However, in all four panels, the Öpik’s Law distribution of separations shown by the solid horizontal line requires a lower mass cutoff  $M_{low} > 1\text{--}3 M_{\odot}$ . The probabilities that the simulated data agree with the observations drop to below 40% at  $M_{low} < 1 M_{\odot}$  for  $\beta < 0$ . The probabilities at low  $M_{low}$  are somewhat higher in the left column ( $r_{in} = 0.02$  AU), but we argue previously that such small inner limits, coupled with such small  $\beta$  are highly improbable physically. Binary fractions  $F < 1$  would only exacerbate the problem, requiring even larger lower mass cutoffs to the Miller & Scalo (1979) IMF. We conclude that the data are grossly inconsistent with a Miller & Scalo (1979) type IMF extending below 2–4  $M_{\odot}$  for any plausible distribution of separations.

We tested whether a Miller & Scalo (1979) type IMF might be made more consistent with the data by the addition of a “twin” component in the same manner described previously. Figure 16 shows a 3x3 grid of contour probability plots similar to Figure 15 except that 25% of the stars are now “twins” with  $q = 0.95\text{--}1.0$  with mean separations  $\langle r_{Twin} \rangle = 3.9 \text{ AU}$  and a log-normal distribution having width  $\sigma_{\log r} = 0.6$ . The highest contours peak in excess of 60%, but these regions lie above lower mass cutoffs of  $M_{low} = 0.8 M_{\odot}$  for plausible values of  $r_{in} \geq 0.063 \text{ AU}$ . The Öpik’s Law distribution of separations would require  $M_{low} \geq 0.5 M_{\odot}$  where it intersects the peak contour ridge. Even if 25% of the companions are twins, a secondary star mass function similar to the Miller & Scalo (1979) IMF must have a lower mass cutoff at relatively large masses in order to produce the velocity distribution in the data. The implied type Ib/c supernova fractions are  $f_{Ib/c} \geq 0.35$  for the most plausible radial boundary limits (middle and upper-middle panels), at the upper end of currently measured ranges (Li et al. 2007; Leaman et al. 2007).

We tested the Miller & Scalo (1979) type IMF against the data with a “twin” fraction of  $T_{frac} = 0.40$ , similar to the prescription of Pinsonneault & Stanek (2006). Figure 17 shows a 3x3 grid of contour probability plots similar to Figure 16 for this series of Monte Carlo comparisons. The highest contours exceed 60% over a wide area and approach 70%. In nearly all panels, they extend down to cutoff masses of  $\sim 0.1 M_{\odot}$ . In particular, the four upper-right panels having  $r_{in} \geq 0.063 \text{ AU}$  and  $r_{out} \geq 1000 \text{ AU}$  show that the Öpik’s Law distribution of separations intersects the ridge of peak contours in the range  $0.1\text{--}0.3 M_{\odot}$ , i.e., in the range where the Miller & Scalo (1979) type IMF is flat, or turns over for the lowest mass stars. The implied type Ib/c supernova fractions are  $f_{Ib/c} \geq 0.35$  for these panels, at the upper end of, but consistent with, the currently measured values (Li et al. 2007; Leaman et al. 2007).

#### 4.5. Limitations of the Modeling

In order to compare the observations to the modeled velocity distributions we have made a number of simplifying assumptions. Some of these assumptions may account for the result that the best models agree with the data at only the 60–70% level. Nevertheless, we contend that none of these assumptions affect the major conclusions.

We assume that all orbits are circular. Although this is unlikely to be the case for the majority of systems, it provides a reasonable way to estimate the mean properties of an ensemble of systems with a minimum of free parameters, especially in the absence of well-sampled velocity curves that would be required to measure eccentricities. It is also a reasonable approximation for close, massive binaries where the orbits are likely to have circularized.

Early-type systems with periods less than several days are observed to have eccentricities near zero (Giuricin et al. 1984) as are systems with large fractional radii,  $R_*/r > 0.24$  where  $r$  is the semi-major axis and  $R_*$  the stellar radius (North & Zahn 2003; Pan et al. 1998; Zahn 1977). Low-mass binary systems have eccentricities near zero for periods shorter than  $\sim 11$  days (Meibom & Mathieu 2005). Without additional data to provide secure periods for much for our sample, we can only say that at least  $\sim 10$  systems appear to be in such short period orbits. Furthermore, although the velocity amplitude for a primary star in an eccentric system is larger by a factor  $\sqrt{(1 - e^2)}$  compared to a circular system of the same semi-major axis, the rms velocity dispersion averaged over the orbit is smaller by the same factor because the relative radial velocity variations are small over most of the orbital period. It follows that the systematic effects of eccentric orbits cancel to zeroth order and can be neglected unless the majority of systems are highly eccentric.

We assume that each primary star has a single companion that dominates the observed primary kinematics. In reality, triple and quadruple systems probably exist among the sample, but they are likely to be a small fraction of all systems. Among solar type stars the fraction of triple and quadruple systems is  $\leq 4\%$  (Duquennoy & Mayor 1991). The tertiary components, if any, are statistically likely to have wide orbital separations and long periods, making their observable dynamical influence minimal over few year time baselines and at  $\sim 10 \text{ km s}^{-1}$  velocity precisions.

We assume that the measured velocity variations are due to orbital dynamics of the primary star. Stellar photospheric line profile variations may be present among some of the most massive stars, especially the evolved stars in our sample (31 of 114 or about 27% are post-main-sequence stars). Line profile variations attributed to atmospheric pulsations are observed in  $\geq 77\%$  of evolved O stars and in some Be stars (Penrod 1986; Vogt & Penrod 1983) but rarely among dwarfs (Fullerton et al. 1996). These phenomena could mimic the effects of bona fide orbital velocity variability in systems observed with sufficiently high spectral resolution to see these effects. Neglecting this possibility would lead to an overestimate of the binary fraction and bias the conclusions in favor a larger  $\alpha$  and/or smaller  $\beta$ . Since our sample consists predominantly of dwarfs and non-Be stars (there are 3–5 Be stars), the impact of line profile variations is minimal and is unlikely to dominate the results.

Finally, we caution that the binary characteristics within a single OB association may not be representative of the binary properties in other massive starforming regions. The fraction of binaries, the distribution of mass ratios, the initial orbital separations, and their eccentricities may depend upon the *global* conditions in the molecular cloud from which they formed. Garcia & Mermilliod (2001) highlight a possible trend in the binary frequency with cluster density and richness. For example, the dense, massive molecular clouds with densities

$n_e > 10^7 \text{ cm}^{-3}$  which can produce a super star cluster with  $M > 10^6 M_\odot$  within a diameter of a few pc (O’Connell et al. 1994; Elmegreen & Efremov 1997; Kobulnicky & Johnson 1999; Billett et al. 2002) may produce a different population of binaries than those which generate the relatively diffuse OB associations. This would be especially true if binaries result primarily from gravitational encounters between cloud cores and/or massive protostars early in the star formation episode. On the other hand, it might be argued that the production of binaries is primarily a *local* effect driven by physics on the scale of an individual cloud core ( $< 10 \text{ AU}$ ). If massive stars form primarily through mergers of intermediate mass stars in a dense core as suggested by Bonnell et al. (1998), then perhaps characteristics of massive binaries are set by the masses and separations of subclumps that fail to complete the merger process. Krumholz (2006) provides a review of the predictions and consequences of competing theories for massive star formation.

## 5. Conclusions

We have analyzed the radial velocity data spanning 6 years on a large sample of OB stars from the Cygnus OB2 Association to measure the probable system characteristics among massive binaries. We have compared the radial velocity amplitudes to expectations from Monte Carlo models based upon several popular formulations for the mass ratios distributions in massive binaries. These comparisons highlight the allowed parameter space and the sensitivity of the models to the key binary parameters: the true binary fraction,  $F$ ; the power-law slope  $\alpha$  of the mass ratio distribution over the range  $q_{low} < q < 1.0$ ; and  $\beta$ , the power law slope of the orbital separations between the inner and outer radial boundaries,  $\log(r_{in})$  and  $\log(r_{out})$ . The data improve upon prior studies by including a larger number of objects in a common association over more observational epochs. The sample also consists of a young population with a (mostly) uniform age of 2–3 Myr, thereby minimizing evolutionary and selection effects inherent in many samples.

1. Descriptions of the massive binary mass ratio distribution and orbital separation distribution derived from spectroscopic and direct imaging studies are biased by selection effects and measurement limitations. These produce apparently conflicting prescriptions of massive binary parameters. Power-law parameterizations require explicit boundaries over which the power law is valid. These boundaries are often insufficiently well specified in the published studies to allow meaningful comparisons given that the conclusions are sensitive to the choice of  $r_{in}$  and  $r_{out}$ , as shown in the Figures herein.
2. Radial velocity amplitude data, such as we model here, are consistent with a range of mass ratio distributions and orbital radius distributions. Although the models are

degenerate in  $\alpha$  and  $\beta$ , the best fitting power-law slopes are correlated. Under the assumption that the distribution of orbital separations is approximately flat (Öpik's Law  $\equiv \beta = 0$ ), the data allow only a narrow range of  $\alpha$  for given inner and outer radial boundaries.

3. Power-law parameterizations of  $f(q)$  and  $f(r)$  for plausible boundary values  $q_{min} = 0.02$ ,  $0.063 \text{ AU} < r_{in} < 0.200 \text{ AU}$ ,  $r_{out} = 10000 \text{ AU}$ , and  $F = 1.0$  are consistent with a mass ratio distribution described by  $-0.6 < \alpha < 0.0$  assuming that  $\beta \simeq 0$ , i.e., the flat Öpik's Law distribution of separations. This is consistent with  $\alpha \simeq -0.4$  reported for adaptive optics imaging studies of Sco OB2 (Kouwenhoven et al. 2005; Kouwenhoven 2006). Best-fitting Monte Carlo Models are, on average, consistent with the data at the  $P_a = 60\text{--}70\%$  level. Agreement between models and data is limited by discrepancies between the cumulative distribution functions of the model velocity amplitudes and the data both at small velocities  $V_h \sim 20 \text{ km s}^{-1}$  and at large velocities  $V_h \sim 80 \text{ km s}^{-1}$  in roughly equal proportions. This result suggests that small sample size, measurement uncertainties, and the possible presence of higher-order systems in the data all act to preclude better agreement.
4. Power-law models with binary fractions  $F = 0.8$  fit the data slightly more poorly than models with  $F = 1.0$ , and they require larger mean mass ratios with  $-0.4 < \alpha < 1.0$ .
5. Power-law models with binary fractions  $F \leq 0.6$  fit the data significantly less well, having  $P_a < 0.4$ . They also require extreme values of  $\alpha$ ,  $\beta$ , and  $f_{Ib/c} < 0.20$  that are inconsistent with observational studies.
6. The Hogeveen (1992) distribution of mass ratios ( $\alpha = -2$  for systems with  $q > 0.3$  and  $\alpha = 0$  for systems with  $q < 0.3$ ) for  $r_{in} = 0.063 \text{ AU}$  and  $r_{out} = 1000 \text{ AU}$  can reproduce the data at the  $\sim 60\%$  level, comparable to the best-fitting power-law models with  $\alpha \simeq -0.6$ . This is because the two-component Hogeveen (1992)  $q$  distribution effectively mimics a power law with slope intermediate between  $-2$  and  $0.0$ . Given the ad hoc nature of the this formulation, its additional parameters, and its inability to produce a superior match to the data, we find no reason to prefer it over a simpler power-law description for  $f(q)$ .
7. Secondary star masses drawn from a Miller & Scalo (1979) IMF are inconsistent with the data unless the IMF is truncated at low masses below  $\sim 2\text{--}4 M_\odot$ . IMF truncation at such high masses is required to produce the levels of velocity variability seen in the data. *The implication here is that the physical conditions under which massive stars form are conducive to producing relatively close binaries with correlated component masses.*

8. Mass ratio distributions involving both a twin component comprising 25–40% of multiple systems and a power-law component with  $f(q) \propto q^0$  (i.e., flat) for the remainder of multiple systems (Pinsonneault & Stanek 2006) are inconsistent with the data unless the true binary fraction is  $F \leq 0.60$ . Such low binary fractions are shown to be improbable. However, mass ratio distributions involving both a twin component comprising  $\sim 40\%$  of multiple systems and a power-law component with  $\alpha = -2 \text{ --- } -3$  (i.e., Salpeter-like) are consistent with the data.
9. Secondary star mass distributions comprised of two components, a power-law component and a “twin” component with  $q > 0.95\%$ , provide good agreement with the data at the level of  $\sim 70\%$ , marginally better than the best-fitting single power-law models. If the fraction of twin systems is  $T_{frac} = 25 - 40\%$  and these secondaries have mean orbital separations  $< \log[r(AU)] > = 0.6 \pm 0.6$ , then the data are consistent with the remainder of the companions being drawn from the canonical Miller-Scalo -type field star IMF. This formalism simultaneously predicts a type Ib/c supernova fraction of  $f_{Ib/c} = 0.30 - 0.40$ , consistent with the most recent estimates. *This two-component description may allow for the production of massive binary phenomena such as the large number of double neutron star systems that seem to be required by the data (see Kalogera et al. 2007, for a review) while simultaneously permitting the production of low-mass X-ray binaries at the expected rates.*
10. The best-fitting binary parameters also predict that the fraction of core-collapse supernovae that are type Ib/c supernovae is least 30% (assuming single stars do not produce type Ib/c supernovae). If the actual Ib/c supernova fraction were 15%, the allowed binary parameter space would require binary systems where the two components were all nearly the same mass (high  $\alpha$ ) and with orbital separations well above Öpik’s law ( $\beta \gtrsim 1$ ). Such values, although possible, seem unlikely. More likely is that the binary observations indirectly support the most recent supernova observations suggesting that the Ib/c supernova fraction may be as high as 30–40%.

Observational work that better defines the distribution of binary separations, mass ratios, and binary fractions will help to reduce degeneracies in the types of model constraints used here. Thereby, such data will allow a more precise specification of initial binary parameters. Optical interferometric observations of companions to massive stars in the radial range  $< 20 \text{ AU}$  would help verify that the Öpik’s Law distribution of separations extends to smaller orbital distances. Such data may also begin to directly identify “twin” systems with typical separations  $\sim 1\text{--few AU}$ . The continuing Cyg OB2 radial velocity survey (Kiminki et al. 2007) will also measure orbital parameters, modulo inclinations, for a sizable sample of mas-

sive binaries with a common origin, permitting tighter constraints on the binary separations and companion masses.

We thank the time allocation committees of the Lick, Keck, WIYN, and WIRO Observatories for generous observing allocations and Stan Woosley for making this project possible. We acknowledge helpful conversations with Peter Conti, Steve Vogt, Laura Penny, Bob Mathieu, Doug Gies, and Ed van den Heuvel. We acknowledge Dan Kiminki for his assistance with the Cygnus OB2 survey data in the preparation of this manuscript. We thank the referee, Ronald Webbink, for his substantial investment of time on comments that greatly improved this paper. We are grateful for support from the National Science Foundation through the Research Experiences for Undergraduates (REU) program grant AST-0353760 and through grant AST-0307778. The work of C. F. was in part under the auspices of the U.S. Dept. of Energy, and supported by its contract W-7405-ENG-36 to Los Alamos National Laboratory and by National Science Foundation under Grant No. PHY99-07949.

*Facilities:* WIRO (), WIYN (), Shane (), Keck:I ()

## REFERENCES

Abt, H. A., & Levy, S. G. 1976, ApJS, 30, 273

Abt, H. A., & Levy, S. G. 1978, ApJS, 36, 241

Abt, H. A., Gomez, A. E. & Levy, S. G. 1990, ApJS, 74, 551

Abt, H. A. 1983, ARA&A, 21, 343

Batten, A. H., Fletcher, J. M., & MacCarthy, D. G. 1989, Eight Catalog of the Orbital Elements of Spectroscopic Binary Systems, Victoria, B.C.

Belczynski, K. Kalogera, V., & Bulik, T. 2002, ApJ, 572, 407

Bhattacharya, D., & van den Heuvel, E. P. J. 1991, Phys. Reports, 201, 1

Billett, O. H., Hunter, D. A., Elmegreen, B. G. 2002, AJ, 123, 1454

Blaauw, A. 1961, BAN, 15, 265

Bonnell, I. A., Bate, M. R., & Zinnecker, H. 1998, MNRAS, 298, 93

Cappellaro, E., Turatto, M., Tsvetkov, D. Yu., Bartunov, O. S., Pollas, C., Evans, R., Hamuy, M. 1997, A&A, 322, 431

Cappellaro, E., Evans, R., & Turatto, M. 1999, A&A, 351, 459

Duquennoy, A. & Mayor, M. 1991, A&A, 248, 485

Eggleton, P. P., Fitchett, M. J., & Tout, C. A. 1989, ApJ, 347, 998

Elmegreen, B. G., & Efremov, Y. N. 1997, ApJ, 480, 235

Fisher, J., Schröder, K.-P., & Smoth, R. C. 2005, MNRAS, 361, 495

Fryer, C. L., Burrows, A., & Benz, W. 1998, ApJ, 496, 333

Fryer, C. L., & Woosley, S. E. 1998, ApJ, 502, L9

Fryer, C. L., Woosley, S. E., & Hartmann, D. H. 1999, ApJ, 526, 152

Fryer, C. L., Rockefeller, G., Hungerford, Aimee, & Melia, F. 2006, ApJ, 638

Fullerton, A. W., Gies, D. R., & Bolton, C. T. 1996, ApJS, 103, 475

Garmany, C. D., Conti, P. S., & Massey, P. 1980, ApJ, 242, 1063

Garcia, B. & Mermilliod, J. C. 2001, A&A, 368, 122

Gies, D. R. 1987, ApJS, 64, 545

Giuricin, G., Mardirossoan, F., & Mezzetti, M. 1984, A&A, 134, 365

Goldberg, D., & Mazeh, T. 1994, A&A, 282, 801

Halbwachs, J. L. 1987, A&A, 183, 234

Halbwachs, Mayor, M., Udry, S., & Arenou, F. 2003, A&A, 397, 159

Hanson, M. M. 2003, ApJ, 597, 957

Harries, T. J., Hilditch, R. W., Howarth, I. D. 2003, MNRAS, 339, 157

Heger, A., Fryer, C. L., Woosley, S. E., Langer, N., Hartmann, D. H. 2003, ApJ, 591, 288

Hillwig, T. C., Gies, D. R., Bagnolo, W. G., Huang, W., McSwain, M. V., Wingert, D. W. 2006, ApJ, in press

Hirschi, R., Meynet, G., & Maeder, A. 2005, A&A, 443, 581

Hogeweene, S. J. 1990, *Ap&SS*, 173, 315

Hogeweene, S. J. 1992, *Ap&SS*, 196, 299

Humphreys, R. M. & McElroy, D. B. 1984, *ApJ*, 284, 565

Jeffers, H. M., Van den Bos, W. H., & Greeby, F. M. 1963, Index Catalog of Visual Double Stars, Lick Observatory, Mount Hamilton

Kalogera, V., & Webbink, R. F. 1998, *ApJ*, 493, 351

Kalogera, V., Beclzynski, K., Kim, C., O'Shaughnessy, R., & Willems, B. 2007, *Phys. Reports.*, 442, 75

Kiminki, D., Kobulnicky, H. A., Kinemuchi, K., Irwin, J. S., Fryer, C. L. Berrington, R. C., Uzpen, B. Monson, A. J., Pierce, M. A., & Woosley, S. E. 2007, *ApJ*, in press

Kobulnicky, H. A. & Johnson, K. E. 1999, *ApJ*, 527, 154

Kouwenhoven, M. B. N., Brown, A. G. A., Zinnecker, H., Kaper, L., & Portegies Zwart, S. F. 2005, *A&A*, 430, 137

Kouwenhoven, M. 2006, PhD Thesis, University of Amsterdam

Krumholz, M. R. 2006, *ASP Conf. Ser.* in press

Krumholz, M. R., McKee, C. F., & Kleim, R. I. 2005, *ApJ*, 618, L33

Kurtz, M. J. & Mink, D. J. 1998, *PASP*, 110, 934

Kroupa, P., Tout, C. A., & Gilmore, G. 1991, *MNRAS*, 251, 293

Kroupa, P., Tout, C. A., & Gilmore, G. 1993, *MNRAS*, 262, 545

Larson, R. B. 2001, *IAU Symp.* 200, 93

Lanz, T., & Hubent, I. 2003, *ApJS*, 146, 417

Lpine, S., & Bongiorno, B. 2007, *AJ*, 133, 889

Leaman, et al. 2007, in preparation

Li, W., Wang, X., Van Dyk, S. D., Cuillandre, J-C., Foley, R. J., Filippenko, A. V. 2007, *astro-ph/0701049*

Lucy, L. B., & Ricco, E. 1979, *AJ*, 84, 401

Lucy, L. B. 2006, A&A, 457, 629

Martins, F., & Schaefer, D., & Hillier, D. J. 2005, A&A, 436, 1049

Mannucci, F., Della Valle, M., Panagia, N., Cappellaro, E., Cresci, G., Maiolino, R., Petrosian, A., Turrat, M., 2005, A&A, 433, 807

Mason, B. D, Gies, D. R., Hartkope, W. I., Bagnolo, W. G., Brummelaar, T., McAlister, H. A. 1998, AJ, 115, 821

Massey, P., Thompson, A.B., 1991, AJ 101, 1408

Mazeh, T., Goldberg, D., Duquennoy, A., & Mayor, M. 1992, ApJ, 401, 265

Meibom, S., & Mathieu, R. D. 2005, ApJ, 620, 970

Miller, G. E., & Scalo, J. M. 1979, ApJS, 41, 513

North, P., & Zahn, J.-P. 2003, A&A, 405, 677

Öpik, E. J., 1924, Tartu Obs. Publ., 25

O'Connell, R. W., Gallagher, J. S. III, Hunter, D. A. 1994, ApJ, 433, 650

Pan, K., Tan, H., & Shan, H. 1998, A&A, 335, 179

Penrod, G. D. 1986, PASP, 98, 35

Petrie, R. M. 1960, Ann. Astrophysics, 23, 744

Pfahl, E. Rappaport, S., Podsiadlowski, P. 2003, ApJ, 597, 1036

Pinsonneault, M. H. & Stanek, K. Z. 2006, ApJ, 639, L67,

Podsiadlowski, Ph., Joss, P. C., Hsu, J. J. L. 1992, ApJ, 391, 246

Podsiadlowski, Ph., Rappaport, S., Pfahl, E. D. 2002, ApJ, 565, 1107

Pourbaix, D., Tokovinin, A. A., Batten, A. H., Fekel, F. C., Hartkopf, W. I., Levato, H., Morrell, N. I., Torres, G., Udry, S. 2006, A&A, 424, 727

Poveda, A., Allen, C., & Parrao, L. 1982, ApJ, 258, 589

Salpeter, E. E. 1955, ApJ, 121, 161

Scalo, J. M. 1986, Fund. Cos. Phys., 11, 1

Scarfe, C. D. 1986, JRASC, 80, 257

Shatsky, N., & Tokovinin, A. 2002, A&A, 382, 92

Tokovinin, A. A., 2000, A&A, 360, 997

Tout, C. 1991, MNRAS, 250, 701

Trimble, V. 1974, AJ, 79, 967

Vogt, S. S., & Penrod, G. D. 1983, ApJ, 275, 661

Wolfire, M. G., & Cassinelli, J. P. 1987, ApJ, 319, 850

Woosley, S. E., Langer, N., & Weaver, T. A. 1995, ApJ, 448, 315

Zahn, J.-P. 1977, A&A, 57, 383

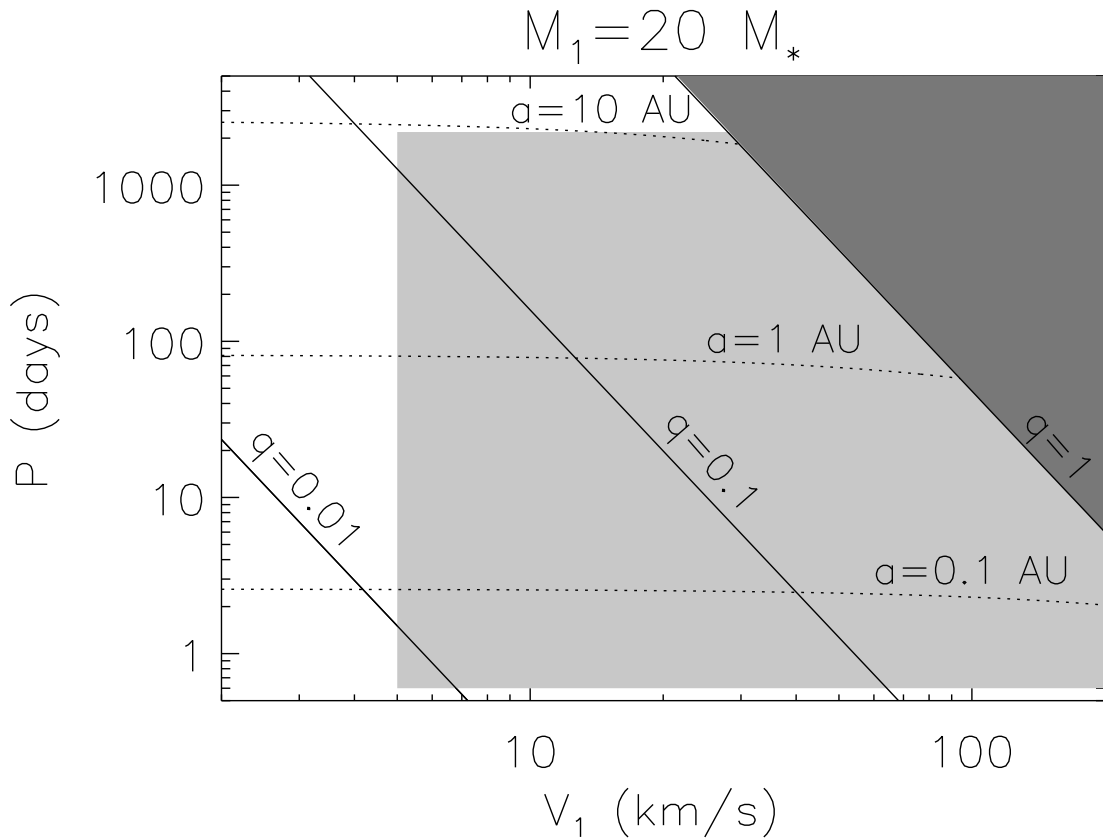


Fig. 1.— Primary star velocity semi-amplitude versus orbital period for binary systems with a  $10 M_\odot$  primary. Solid lines indicate the loci of systems with equivalent mass ratios,  $q \equiv M_2/M_1 = 1.0, 0.1, 0.01$ . Dotted lines indicate loci of systems with common orbital separations,  $r = 0.1, 1.0, 10$  AU. The light gray region indicates the portion of parameter space sampled in this survey. Namely, the data are sensitive to primary velocity amplitudes  $\geq 10$  km s $^{-1}$ , periods shorter than  $\sim 2 \times 6$  years, and orbital separations  $\leq 2 \times 10$  AU.

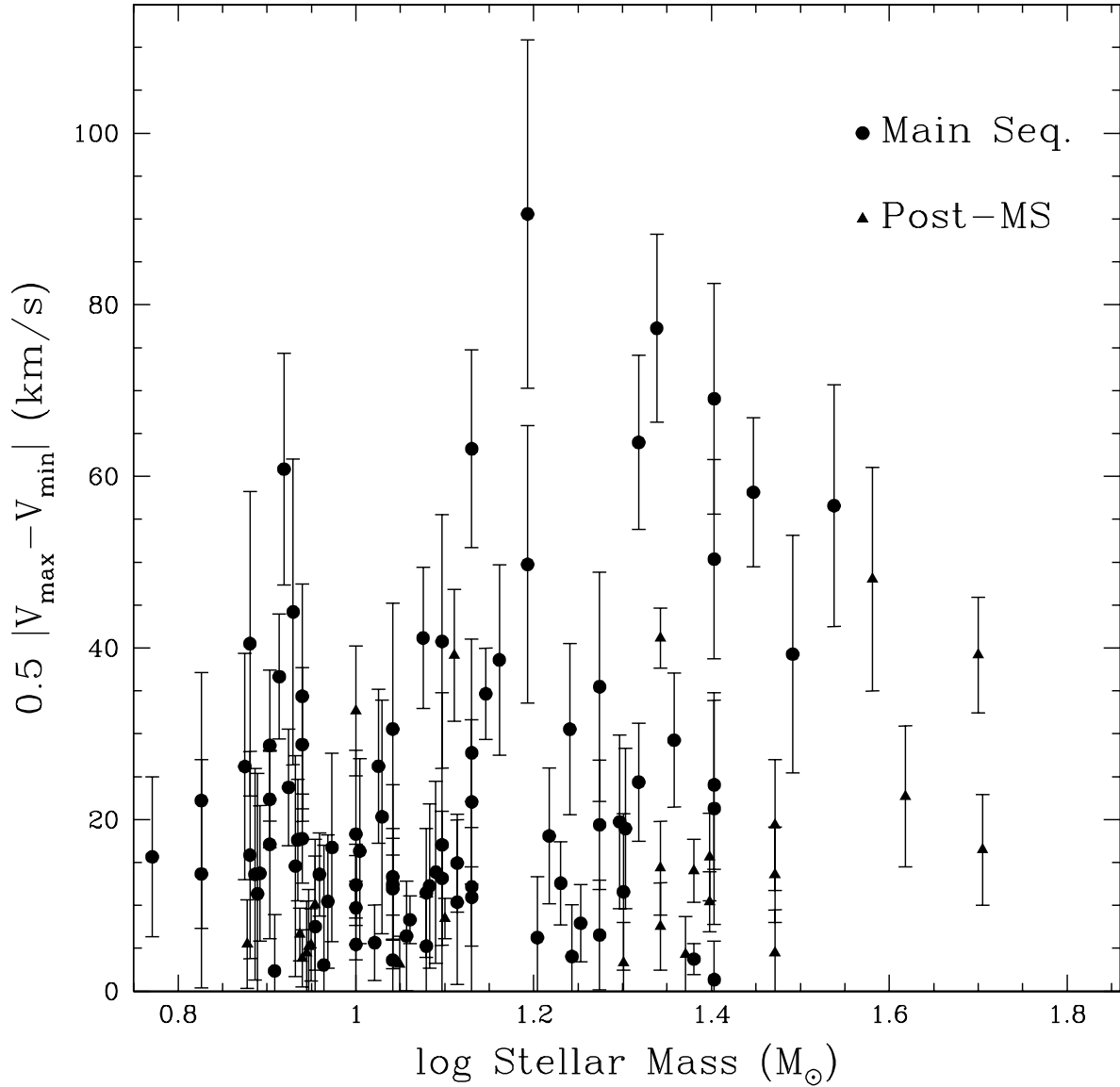


Fig. 2.— Primary star spectroscopic masses versus observed velocity semi-amplitudes,  $V_h \equiv 0.5|V_{\text{max}} - V_{\text{min}}|$ , for the 114 sample stars. Typical uncertainties are  $5-15 \text{ km s}^{-1}$ .

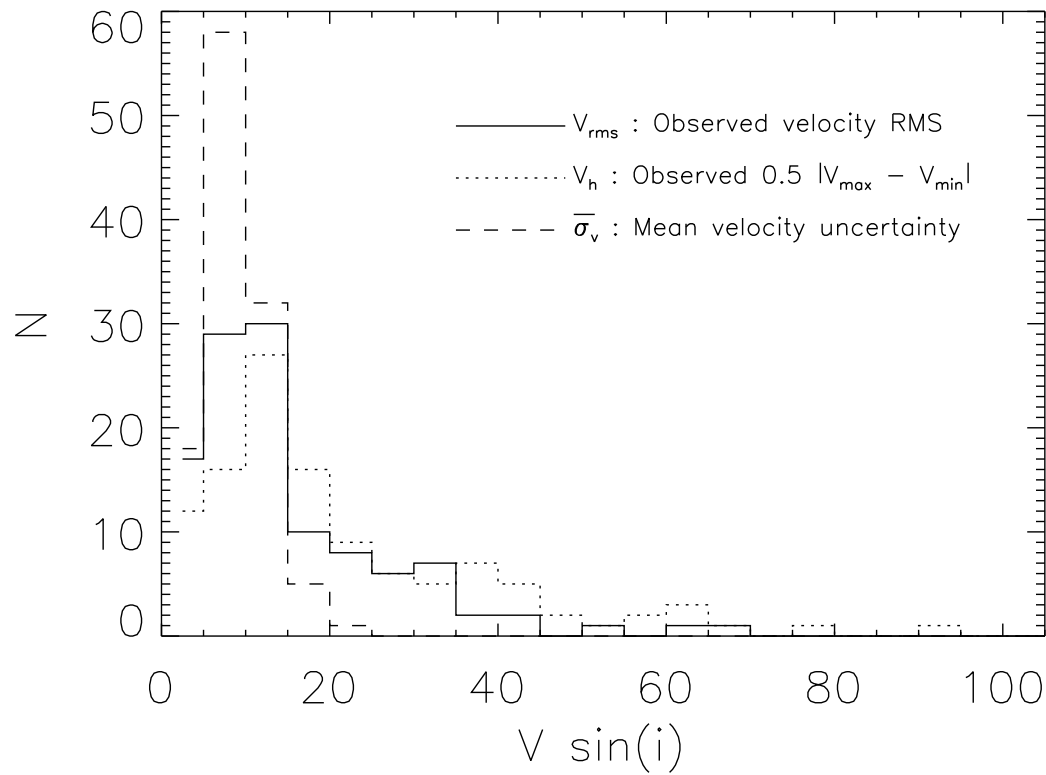


Fig. 3.— The distribution of observed velocity dispersions,  $V_{rms}$  (solid line), velocity semi-amplitudes,  $V_h \equiv 0.5|V_{max} - V_{min}|$  (dotted line), and the mean velocity uncertainties (dashed line) for the sample.

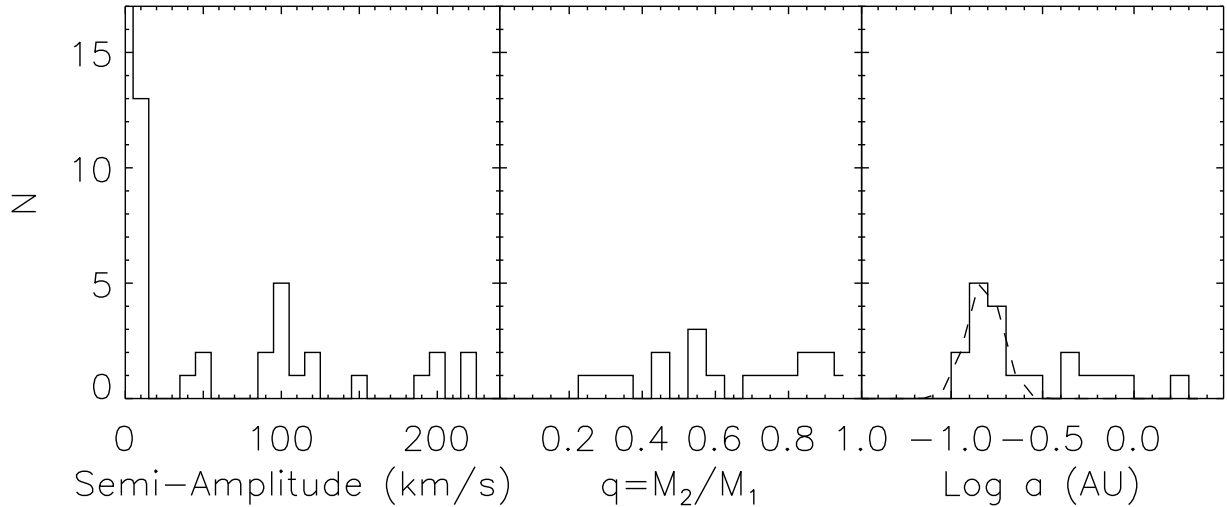


Fig. 4.— *Left panel*: Histogram of the velocity semi-amplitudes for the O stars presented in Table 3 and Figure 1 of Garmany et al. (1980). Note the differences compared to our Figure 3, namely a relative lack of stars in the velocity range 20-80 km s<sup>-1</sup> in the Garmany et al. (1980) sample. *Middle panel*: Histogram of mass ratios,  $q$ , for the O type binaries from Garmany et al. (1980). The histogram is consistent with a flat or rising distribution with increasing mass ratio. *Right panel*: Derived semi-major axis distribution for the O type binary systems from Garmany et al. (1980) assuming an average orbital inclination of 60°. The dashed line is a best fit Gaussian curve which peaks near  $\log(r) = -0.8$  or  $\sim 0.15$  AU with a tail toward larger separations.

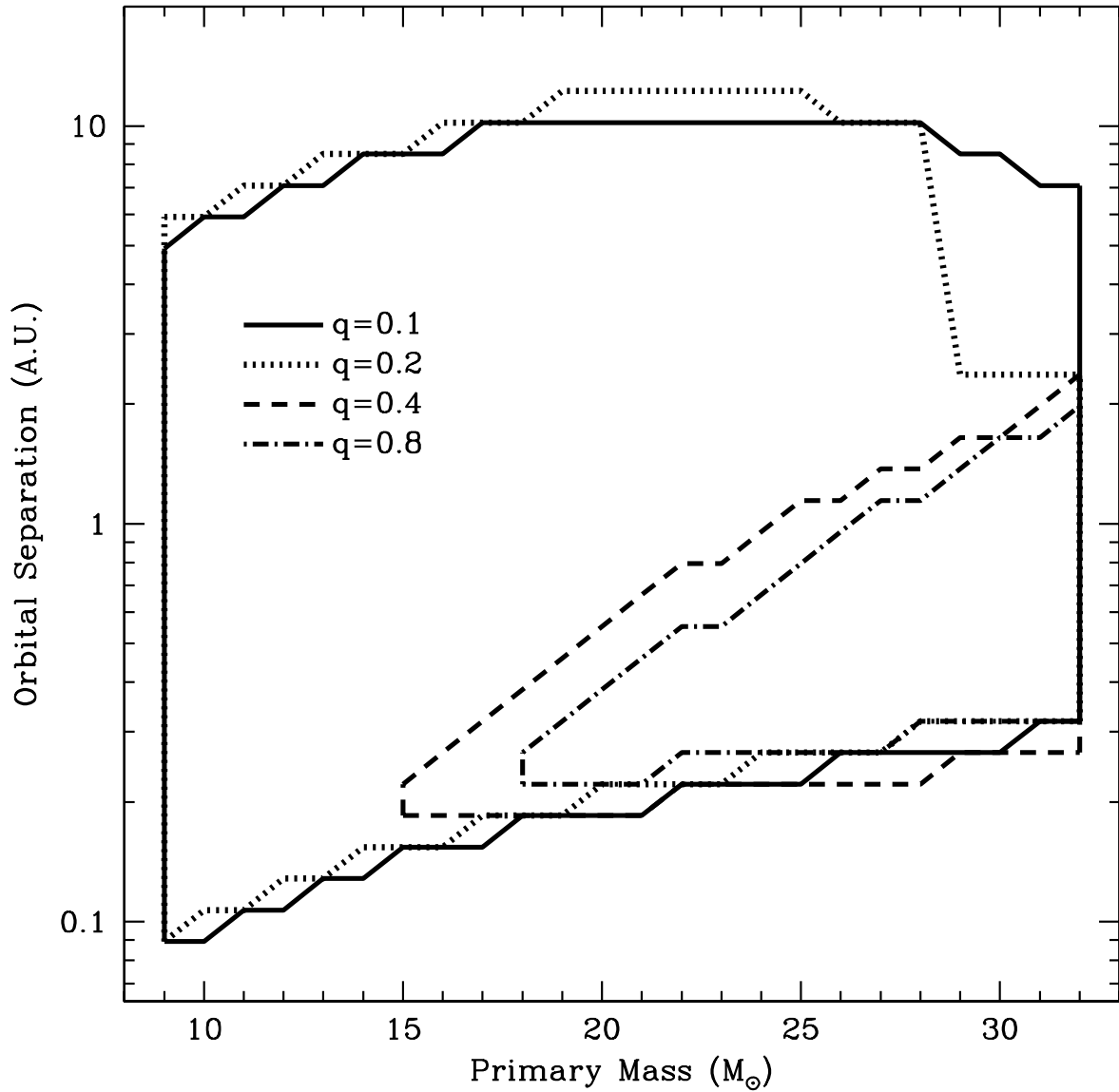


Fig. 5.— Enclosed regions which denote the parameter space of orbital separation and primary mass which produce type Ib/c supernovae for 4 different values of the mass ratio,  $q$ . Type Ib/c supernovae are preferentially made in systems that undergo a common envelope phase, so the parameter space is larger for more extreme mass ratios. Above  $32 M_\odot$ , our wind prescription makes all stars (whether in interacting binaries or not) lose enough mass to become type Ib/c supernovae.

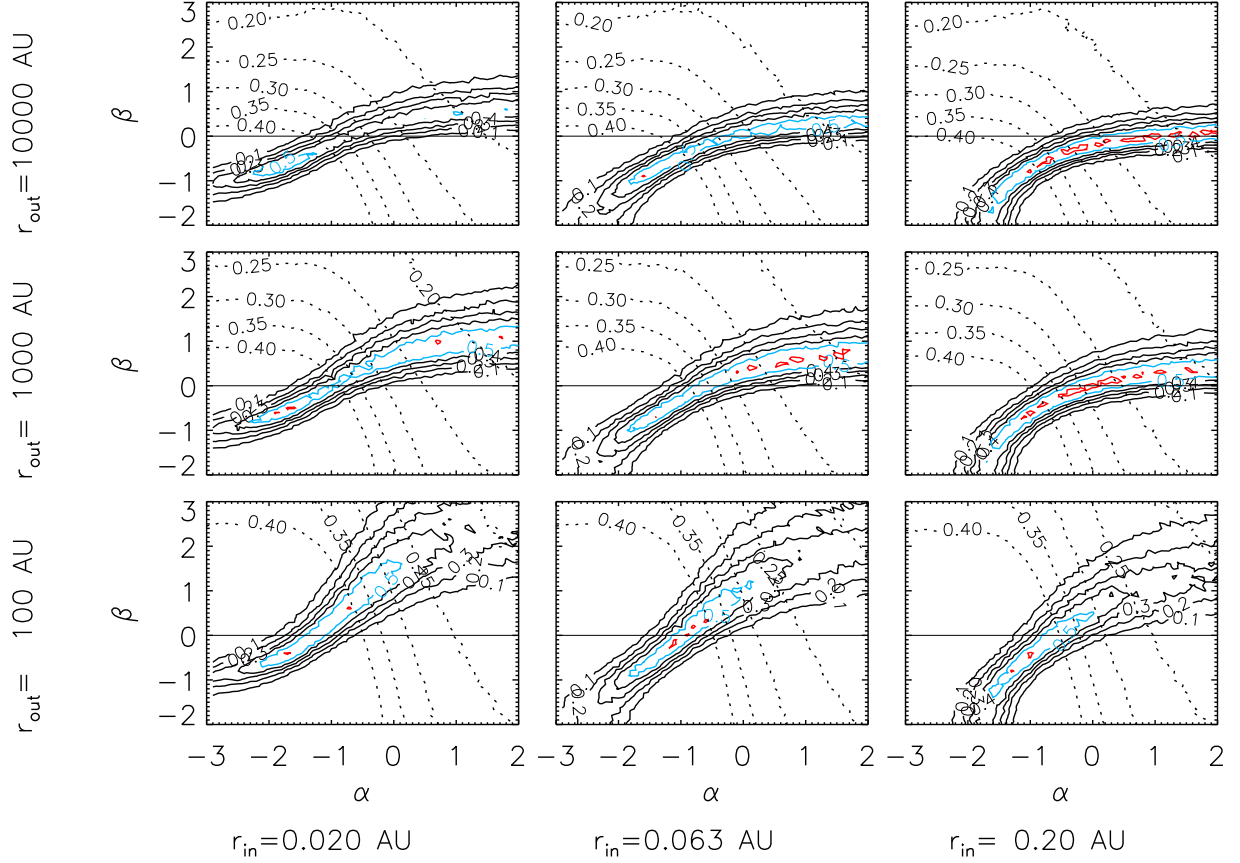


Fig. 6.— Probability contours describing the agreement between the Monte Carlo simulations and the radial velocity data for Cyg OB2 (solid lines) as a function of  $\alpha$  and  $\beta$  in each panel, for a range of minimum orbital radii,  $r_{in}$  (columns), and maximum orbital radii,  $r_{out}$  (rows) with a minimum mass ratio of  $q = 0.02$  and a binary fraction of  $F = 1.0$ :  $r_{in} = 0.020 \text{ AU}$  (left column),  $r_{in} = 0.063 \text{ AU}$  (middle column),  $r_{in} = 0.200 \text{ AU}$  (right column), and  $r_{out} = 10000 \text{ AU}$  (upper row),  $r_{out} = 1000 \text{ AU}$  (middle row),  $r_{out} = 100 \text{ AU}$  (lower row). The horizontal line in each panel marks the nominal  $\beta = 0$  (Öpik's Law) distribution of separations. Contour levels probabilities  $P_a = 10, 20, 30, 40, 50$ , and  $60\%$  likelihood that the simulations and the data are drawn from the same parent population. The  $50\%$  and  $60\%$  contours are colored blue and red, respectively, in the electronic edition of *The Astrophysical Journal*. The most probable values exceed  $60\%$  likelihood and lie along a narrow crescent-shaped ridge line. The dotted contours depict the type Ib/c supernova fraction,  $f_{Ib/c} = 0.10\text{--}0.40$  in increments of  $0.05$ , predicted by Monte Carlo binary population synthesis models (Fryer et al. 1998, 1999).

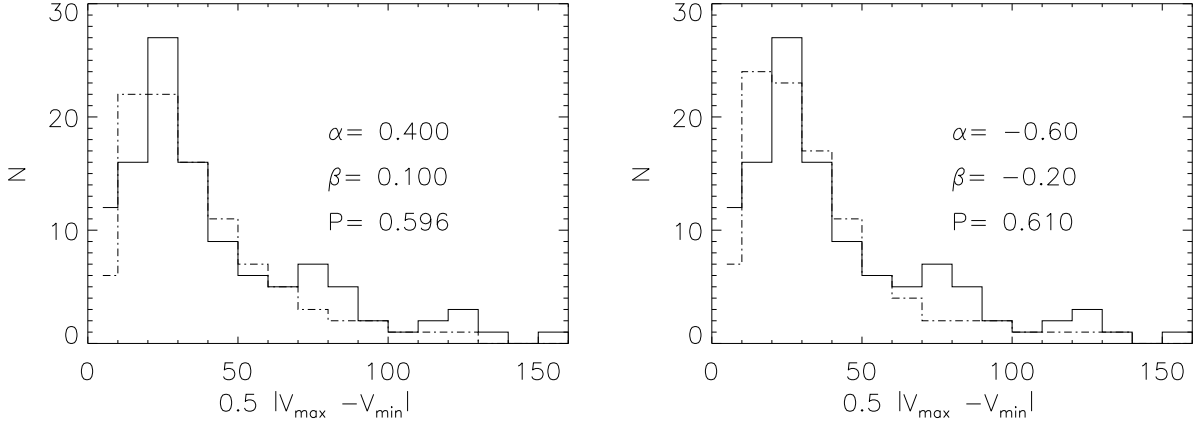


Fig. 7.— Histograms showing the distribution of velocity semi-amplitudes,  $V_h$ , for the data (solid line) and a particular set of Monte Carlo simulations with the indicated values of  $\alpha$  and  $\beta$  (dashed line). Each panel is labeled with the probability,  $P(V_h)$ , that the two histograms are drawn from the same parent population. Both combinations of  $\alpha$ ,  $\beta$  yield probabilities of  $P_a \sim 0.60$  and lie along the ridge line of peak likelihood from the middle-right panel in Figure 6. Either values of  $\beta \simeq 0.10$  paired with  $\alpha \simeq 0.4$  or  $\beta \simeq -0.20$  paired with  $\alpha \simeq -0.6$  provide similarly good matches to the data.

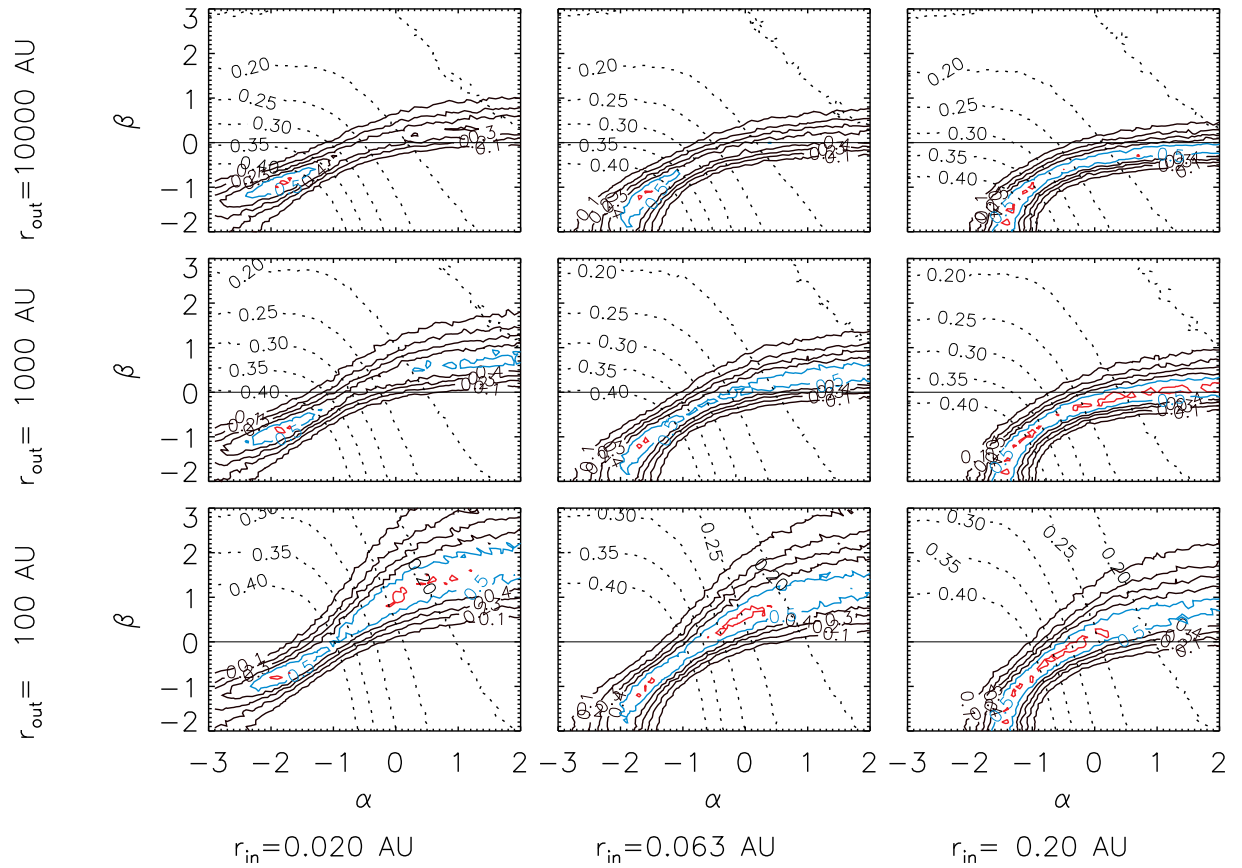


Fig. 8.— Probability contours as in Figure 6 except for a binary fraction of  $F = 0.8$ .

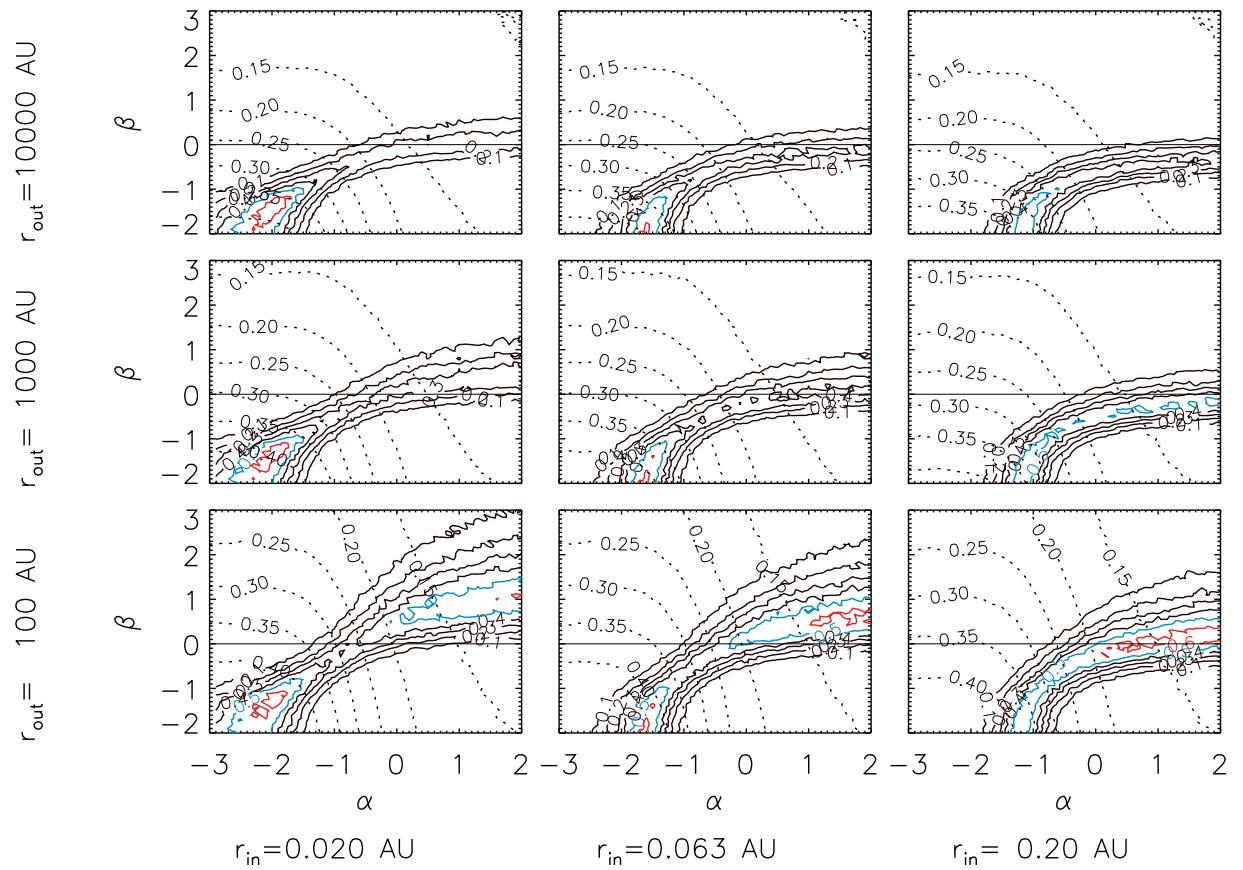


Fig. 9.— Probability contours as in Figure 6 except for a binary fraction of  $F = 0.6$ .

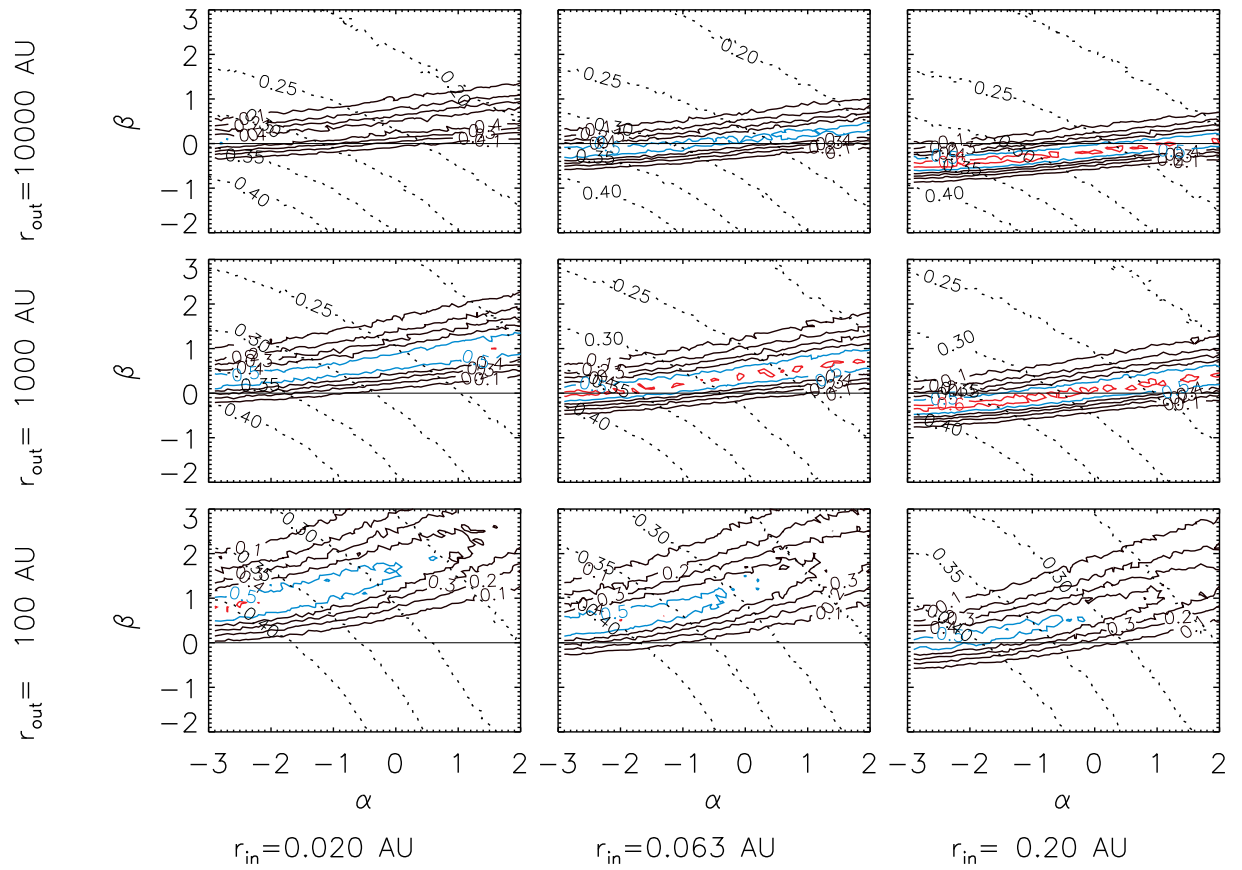


Fig. 10.— Probability contours from Monte Carlo simulations similar to Figure 6 but for the mass ratio distribution given by Hogeveen (1992).

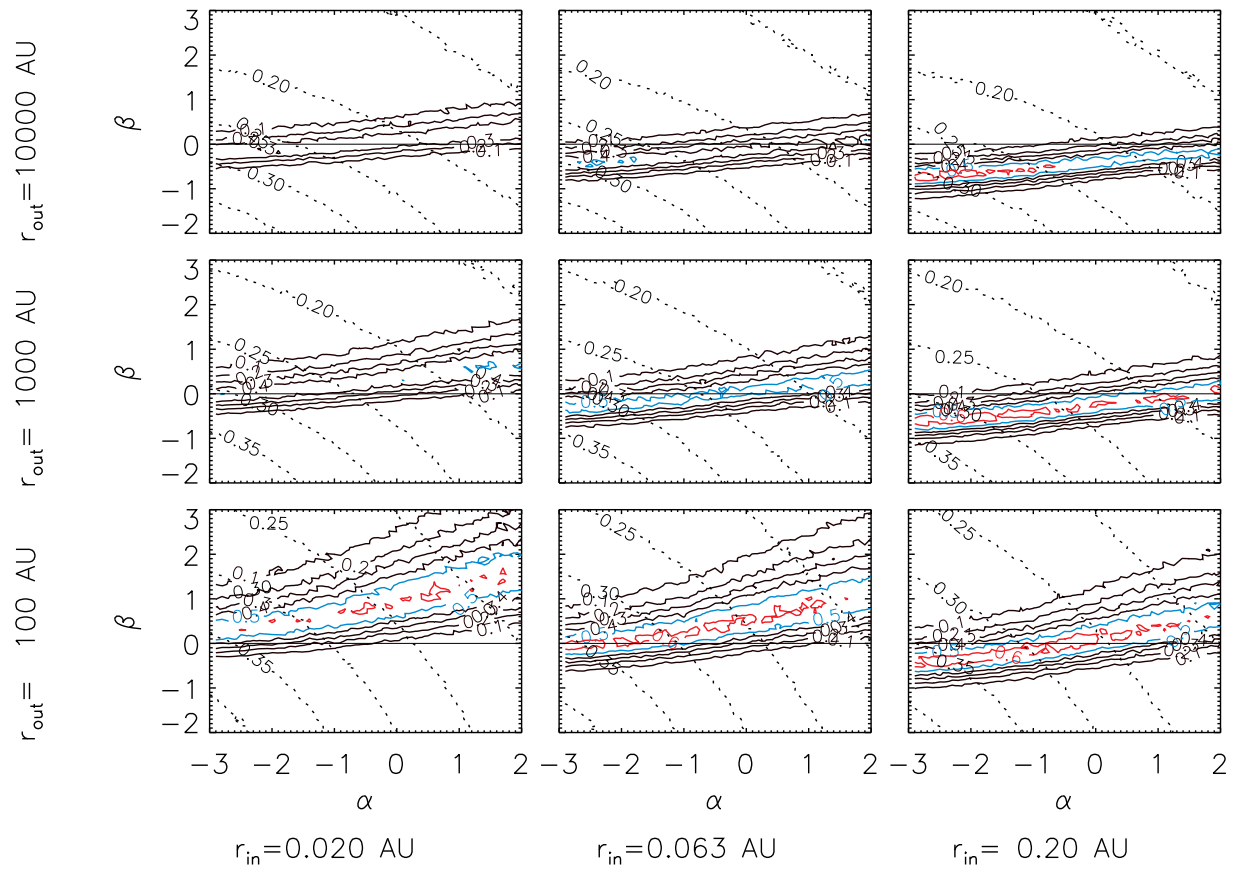


Fig. 11.— Probability contours from Monte Carlo simulations similar to Figure 10 but for a binary fraction of  $F = 0.8$ .

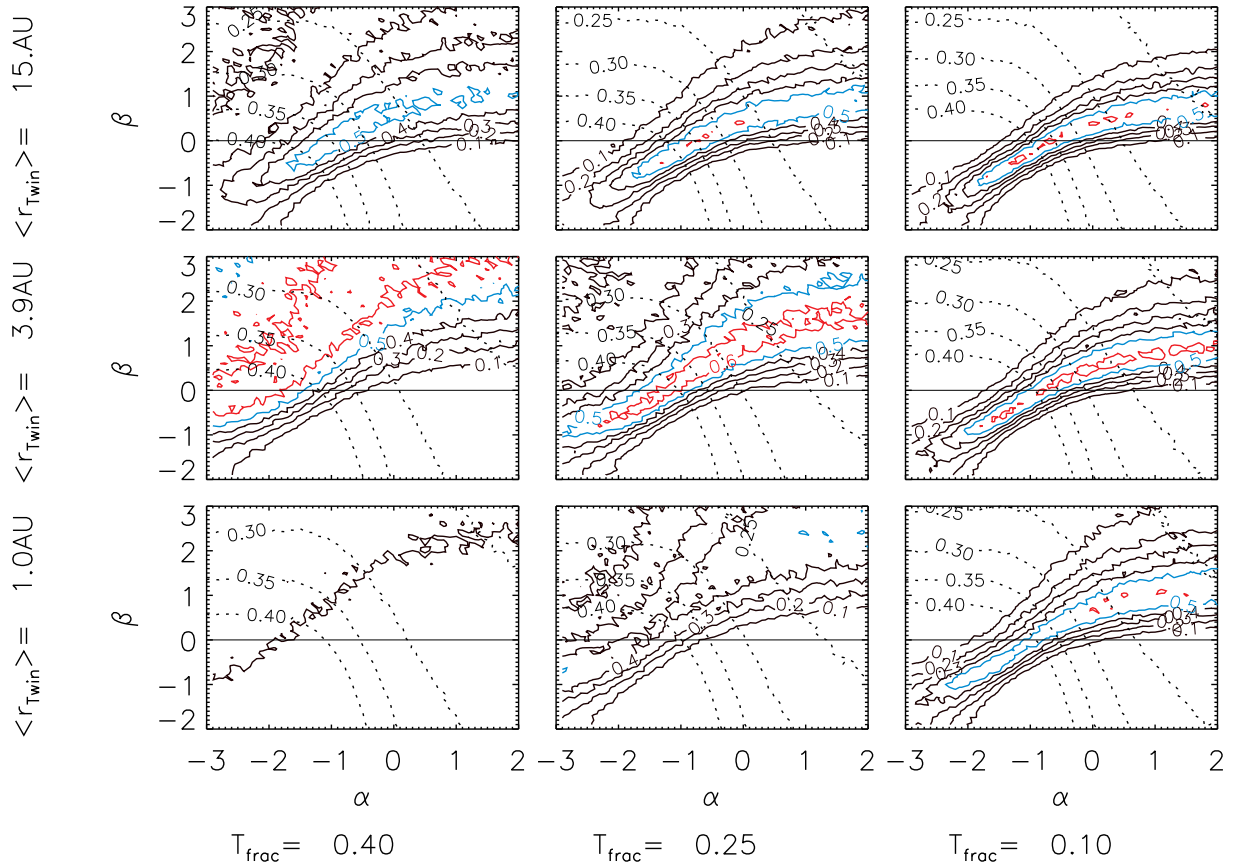


Fig. 12.— Probability contours from Monte Carlo simulations similar to Figure 6 but for a two-component mass ratio distribution. This Figure shows a 3x3 grid of contour probability plots for  $T_{frac}=0.40$  (left column),  $T_{frac}=0.25$  (middle column),  $T_{frac}=0.10$  (right column), and  $\langle r_{Twin} \rangle = 15 AU$  (upper row),  $\langle r_{Twin} \rangle = 3.9 AU$  (middle row),  $\langle r_{Twin} \rangle = 1.0 AU$  (lower row). In all cases, the radial limits for the power-law distribution of the non-twin component are  $r_{in} = 0.063 AU$  and  $r_{out} = 1000 AU$ .

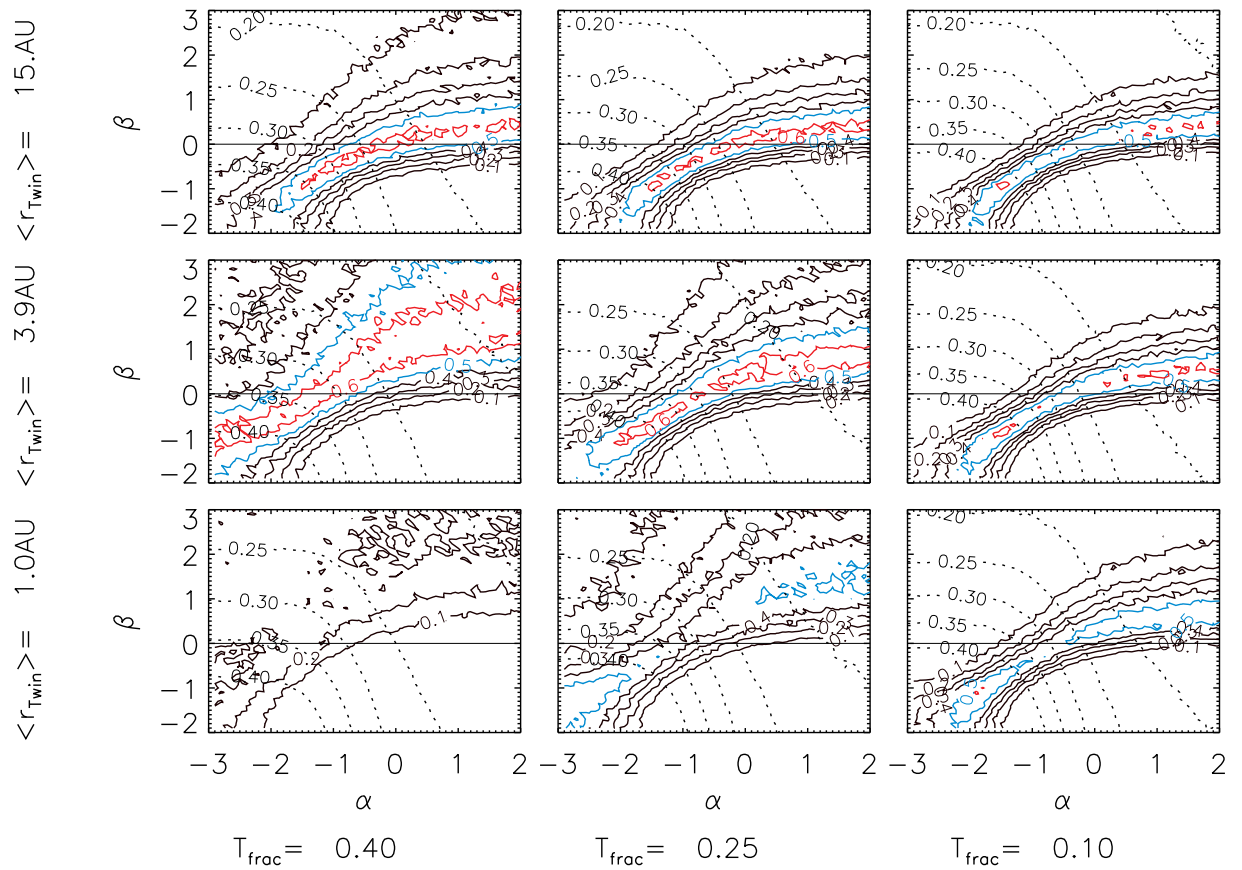


Fig. 13.— Probability contours from Monte Carlo simulations similar to Figure 12 but for a binary fraction  $F = 0.8$ .

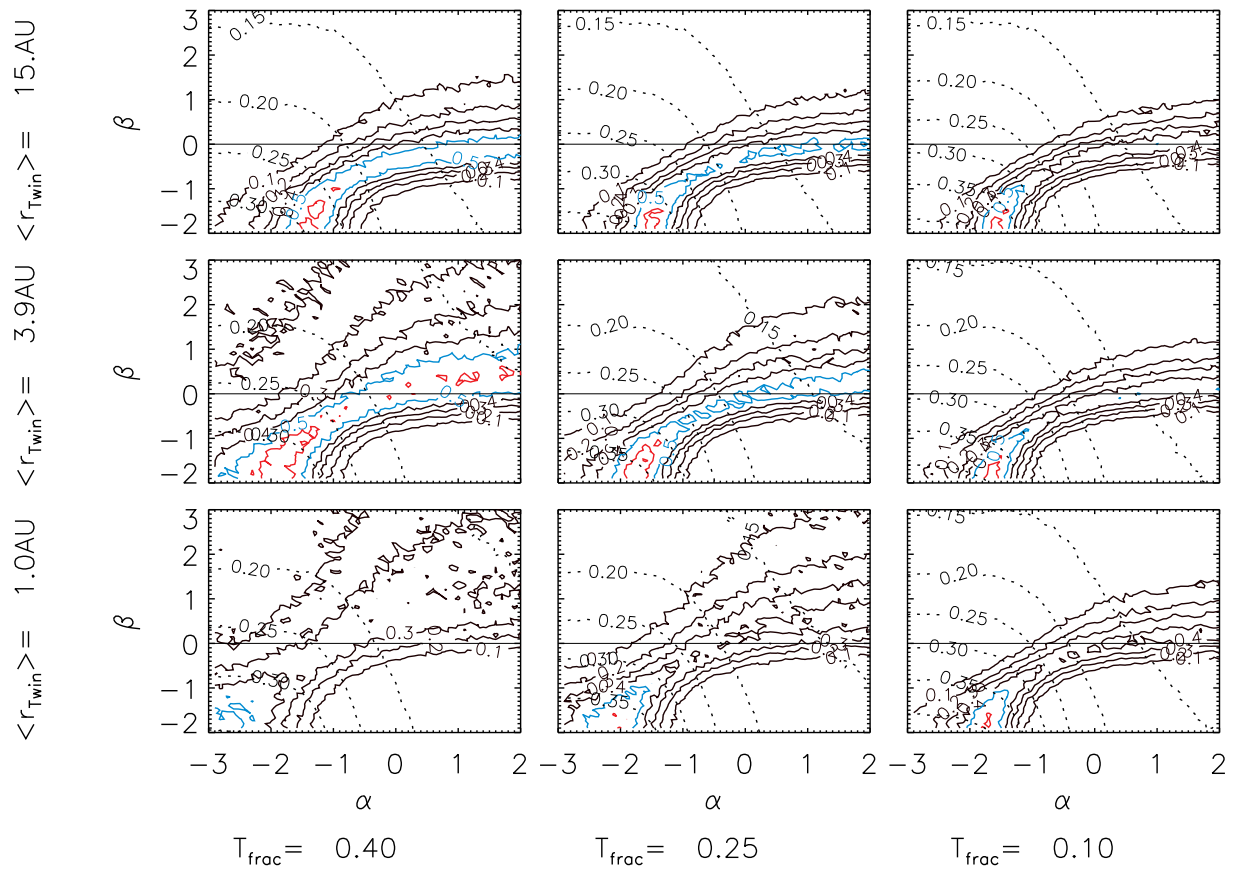


Fig. 14.— Probability contours from Monte Carlo simulations similar to Figure 12 but a binary fraction  $F = 0.6$ .

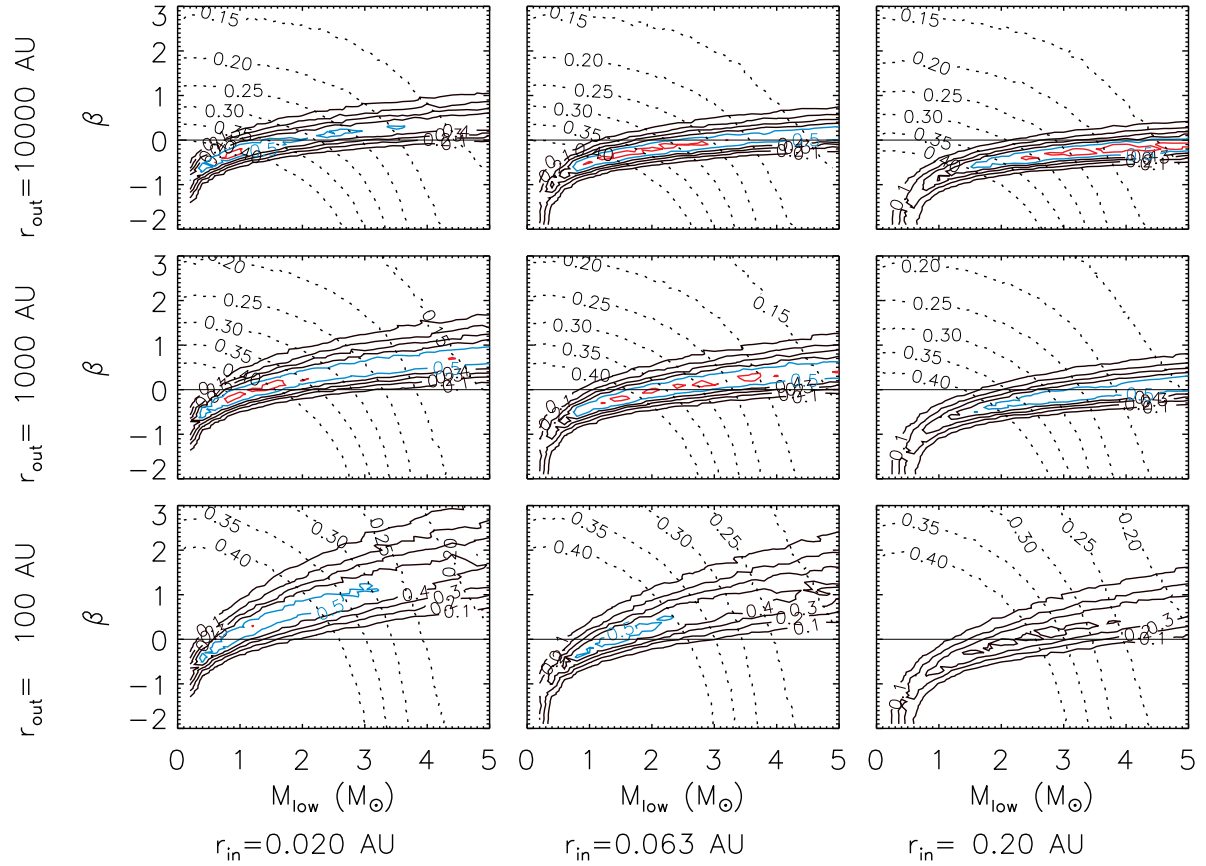


Fig. 15.— Probability contours from Monte Carlo simulations similar to Figure 6 but for a distribution of secondary masses described by the Miller-Scalo IMF with a lower mass cutoff shown on the ordinate of each panel.

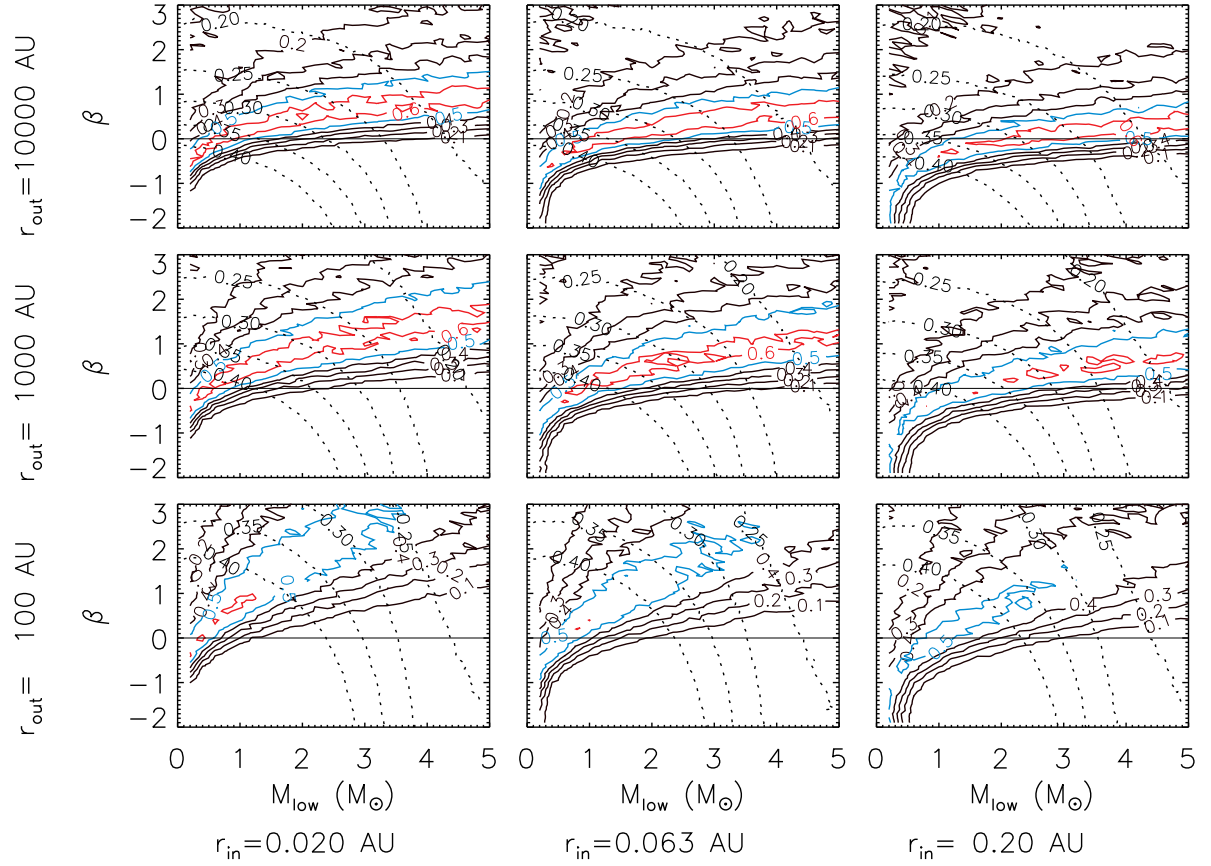


Fig. 16.— Probability contours from Monte Carlo simulations similar to Figure 15 for a distribution of secondary masses described by the Miller-Scalo IMF but with a twin fraction  $T_{frac} = 0.25$ .

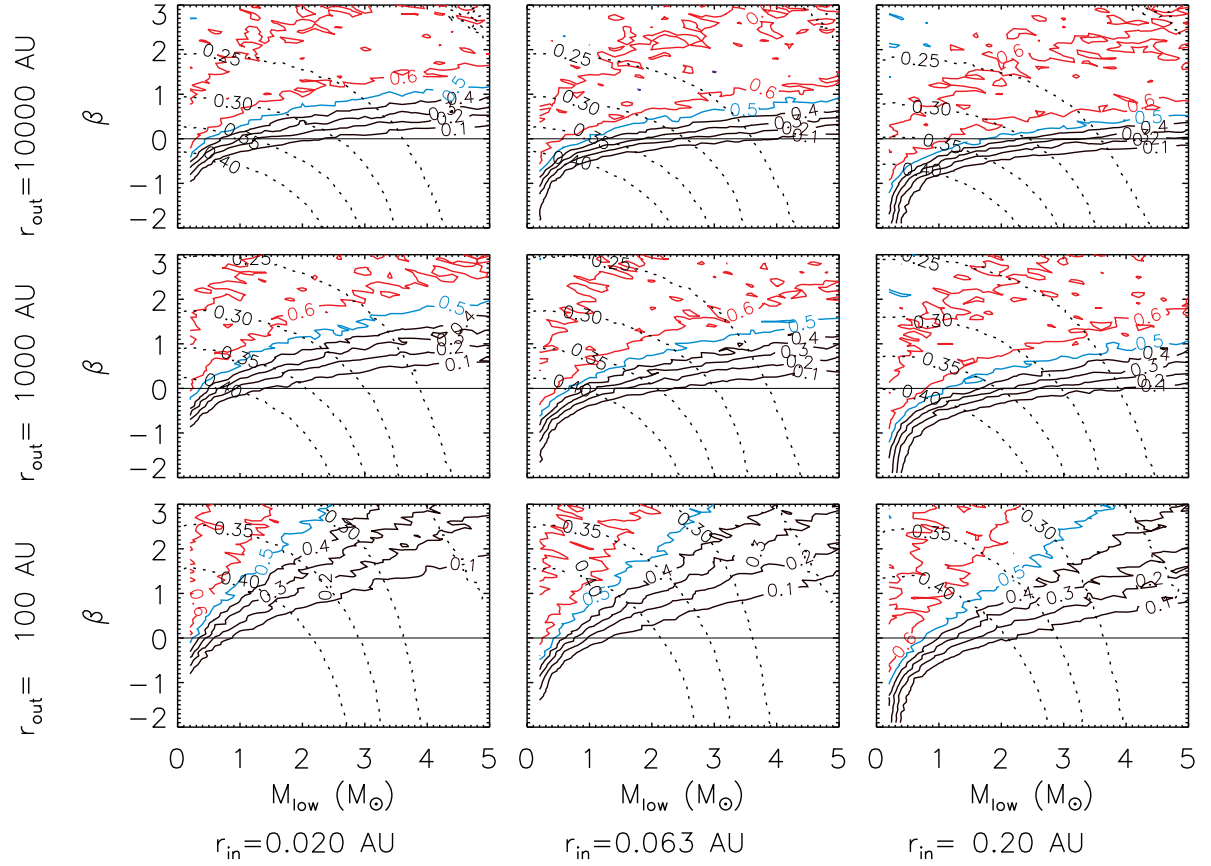


Fig. 17.— Probability contours from Monte Carlo simulations similar to Figure 15 for a distribution of secondary masses described by the Miller-Scalo IMF but with a twin fraction  $T_{frac} = 0.40$ .